Electronic Thesis and Dissertation Repository

7-28-2022 10:30 AM

Characterization of Some Natural Copper samples from the Keweenaw Peninsula of Lake Superior using Electron Microscopy and X-ray Tomography techniques

Emilie MK Landry, *The University of Western Ontario*

Supervisor: Moser, Desmond, *The University of Western Ontario*
Co-Supervisor: Noël, James, *The University of Western Ontario*
A thesis submitted in partial fulfillment of the requirements for the Master of Science degree in Geology
© Emilie MK Landry 2022

Follow this and additional works at: https://ir.lib.uwo.ca/etd

Part of the Geology Commons

Recommended Citation

Abstract

Copper corrosion is of interest to Canada's Nuclear Waste Management Organization as it relates to their multi-barrier system for nuclear waste disposal in deep geologic repositories. Spent fuel canisters coated with a thin copper layer must persist for up to one million years. Natural copper from the Keweenaw Peninsula in Michigan, USA, has persisted for over 1 billion years and is here characterized to understand copper corrosion over geological time. Copper samples representing three rock types were characterized using optical microscopy, scanning electron microscopy techniques (energy dispersive X-ray spectroscopy and electron backscatter diffraction), and micro-computed X-ray tomography (microCT) to establish a workflow and test suitability for a larger study. Energy dispersive X-ray spectroscopy mapping revealed mineralogy and copper paragenesis. This first application of electron backscatter diffraction showed mm-scale grain size and orientation microstructures such as twins. A 3D microCT model revealed hidden domains of high-density phases (e.g., Ag).

Keywords

Summary for Lay Audience

The Nuclear Waste Management Organization of Canada has designed technology to isolate spent nuclear fuel underground in deep geologic repositories for up to 1 million years. The plan is to store the used fuel within steel canisters that have been coated with a thin layer of copper to prevent corrosion of the steel. However, laboratory tests at million year time scales are not practical. In order to investigate the corrosion behaviour(s) of copper over geologic timescales, we looked to natural billion year old copper from the Keweenaw Peninsula in Michigan, USA, which has survived, sometimes un-corroded, for 1 billion years. This study examined three samples from three types of deposits in the region using a suite of imaging techniques to better understand the properties that have resulted in the long-term preservation of natural copper. A scanning electron microscope at Western University was used to obtain elemental and crystallographic (structural) information about the samples. A microCT machine was used to X-ray the samples in 3D to show hidden domains of what is believed to be natural silver within the copper. Together, these imaging techniques allow us to investigate multiple properties of the minerals such as grain size, deformation history, elemental composition, and distribution throughout the sample. This information will be useful in further characterization work done in partnership with corrosion chemists at Western University, and to inform design of NWMO's container coatings to maximize long-term performance.

Acknowledgments

I would like to thank my supervisor Desmond Moser for his help and guidance during this project, and for offering me the opportunity to work on a research project I found deeply engaging and valuable. I would also like to thank Ivan Barker from Surface Science Western for his additional help with teaching me how to run the equipment used during this study, and giving me a better understanding of the analysis techniques used. As well, I wish to thank Arnim Walter, the mineral collector who donated the samples which were used in this study. I also thank the NWMO for funding this research by providing a grant to the research group at Western University. Finally, I would like to thank my parents Bonnie and Mike Landry, who have supported me constantly throughout my academic career and have always been at my side to encourage me.

Table of Contents

List of Tables

List of Figures

<div align="center">Chapter 1</div>

1 Background

A summary of Canada's deep geologic repository plan is presented here, followed by an introduction to the geologic, economic, and cultural history of the copper of the Keweenaw Peninsula. An introduction to the geologic context and likely host rocks of the mines each sample was obtained from is given.

1.1 Background on Canadian Deep Geologic Repositories (DGR)

As the demand for environmentally friendly, low carbon footprint energy grows, and the use of natural gas, oil, and coal decline, sources such as hydroelectricity and nuclear energy are becoming more important. Nuclear energy accounted for 15% of Canadian energy use in 2019 (Natural Resources Canada, 2021), and is a reliable energy source which does not produce CO^2 pollution. A by-product of nuclear energy production is the fuel rods from Canada Deuterium Uranium (CANDU) nuclear reactors. The CANDU rods contain uranium dioxide powder that has been pressed into pellets and then baked into ceramic form. These pellets are then set into zirconium-tin alloy tubes, which are welded together to form the fuel bundles (NWMO, 2021). Spent nuclear fuel pellets produce harmful ionizing radiation in the forms of gamma rays, neutrons, alpha particles, and beta particles (NWMO, 2022), which can have negative impacts on human health in high dosages and must be stored safely (United States Nuclear Regulatory Commission, 2019).

Canada's current plan for nuclear waste disposal is to store used fuel rods in deep geologic repositories (DGRs). These repositories will be located 500 meters underground in a location which has yet to be decided, with the used fuel container (UFCs) being one part of a multi-barrier design system. The UFCs would be placed within highly compacted bentonite clays within either crystalline or sedimentary rock formations (Figure 1) (Hall & Keech, 2017; Fayek & Brown, 2015). The containers are engineered to prevent the leakage of nuclear waste and to ensure safe storage for many thousands of

years at which point ionizing radiation will have declined to background levels. Current plans for the mark II vessel are to use electroplating to create a roughly 3mm layer copper coating to surround a steel interior container that will house the used fuel rods (Hall & Keech, 2017).
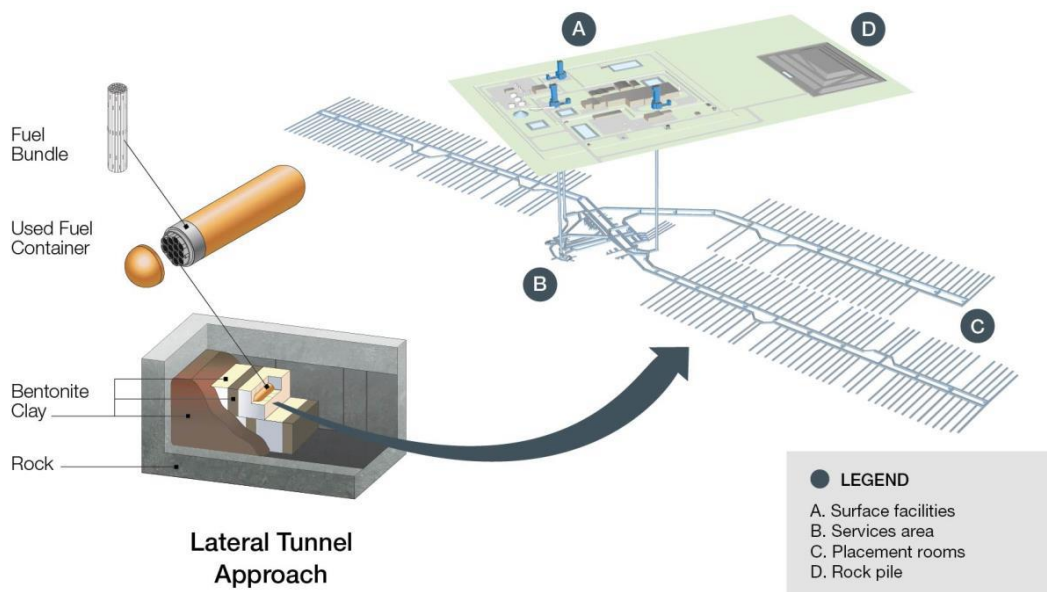
Figure 1: the Nuclear Waste Management Organization's proposed deep geologic repository design (from Dixon, 2019).

The used fuel containers need to isolate nuclear waste from atmospheric and hydrosphere circulation for a minimum of 1,000,000 years according to the NWMO (Scully et al., 2016). Over such long periods of time, there are numerous means that could initiate corrosion that have not yet been investigated (Scully et al., 2016). Corrosion sources include potential defect regions in the copper coatings, the region of the internal steel weld, and corrosion effects within pure water, among others (Hall & Keech, 2017). Corrosion can also be driven by other local sources. Microbially induced corrosion may occur as a result of bacteria within the bentonite clay perhaps metabolizing with the aid of ions created by radiation (Mohd Tadza et al., 2018) The generalized corrosion that will occur as a result requires further research (Abrahamsen-Mills & Small, 2019). Factors such as stress corrosion and the potential effect of glaciation loading onto corrosion have also not been examined and require further investigation (Scully et al., 2016).

Whereas laboratory experiments cannot be conducted on the million-year timescales that the UFCs need to withstand, it is possible to use natural analogues for the purposes of better understanding how copper may respond to corrosion stresses over long periods of time. The copper from the Keweenaw Peninsula that is being examined for this research has resisted corrosion for one billion years under conditions with similarities to those of potential DGR sites within and to the north of the Michigan Basin. In determining a workflow that allows for comprehensive characterization of the natural copper and its depositional settings with multiple microscopy techniques including energy dispersive X-ray spectroscopy (SEM-EDS) and electron backscatter diffraction (SEM-EBSD), we intend to explore the mineral paragenesis, strain history, and chemical composition of the copper and surrounding rock. This will then provide a solid background for further laboratory corrosion work to be done by corrosion chemists at Western University while informing manufacturing designs for NWMO UFC canisters.

1.2   Geologic Background

The Midcontinental Rift (MCR) is a failed continental rift zone in North America that runs through the Keweenaw Peninsula in Michigan (Figure 2). It was at its height in activity around 1100 Ma (Davis & Paces, 1990), forming due to a large mantle plume beneath Laurentia (Green, 1983; Ojakangas et al., 2001). The Portage Lake Volcanics (PLV) that host copper in the Keweenaw Peninsula formed as a result of the MCR, with the alluvial conglomerates seen interbedded with mafic lava flows a result of tectonic derived mass wasting events (Mitchell & Sheldon, 2016). The magmatism which created the rift basalts ended around 1.08 Ga (Bornhorst, 1997), and the copper mineralized after the magmatism events. Radiometric age dating of lithostratigraphic units and dating of minerals such as calcite, intergrown with the natural copper, shows more than 10 million years passing between the end of peak magmatism and the time of natural copper mineralization (Davis & Paces, 1990; Bornhorst et al., 1988; Woodruff et al., 2020).
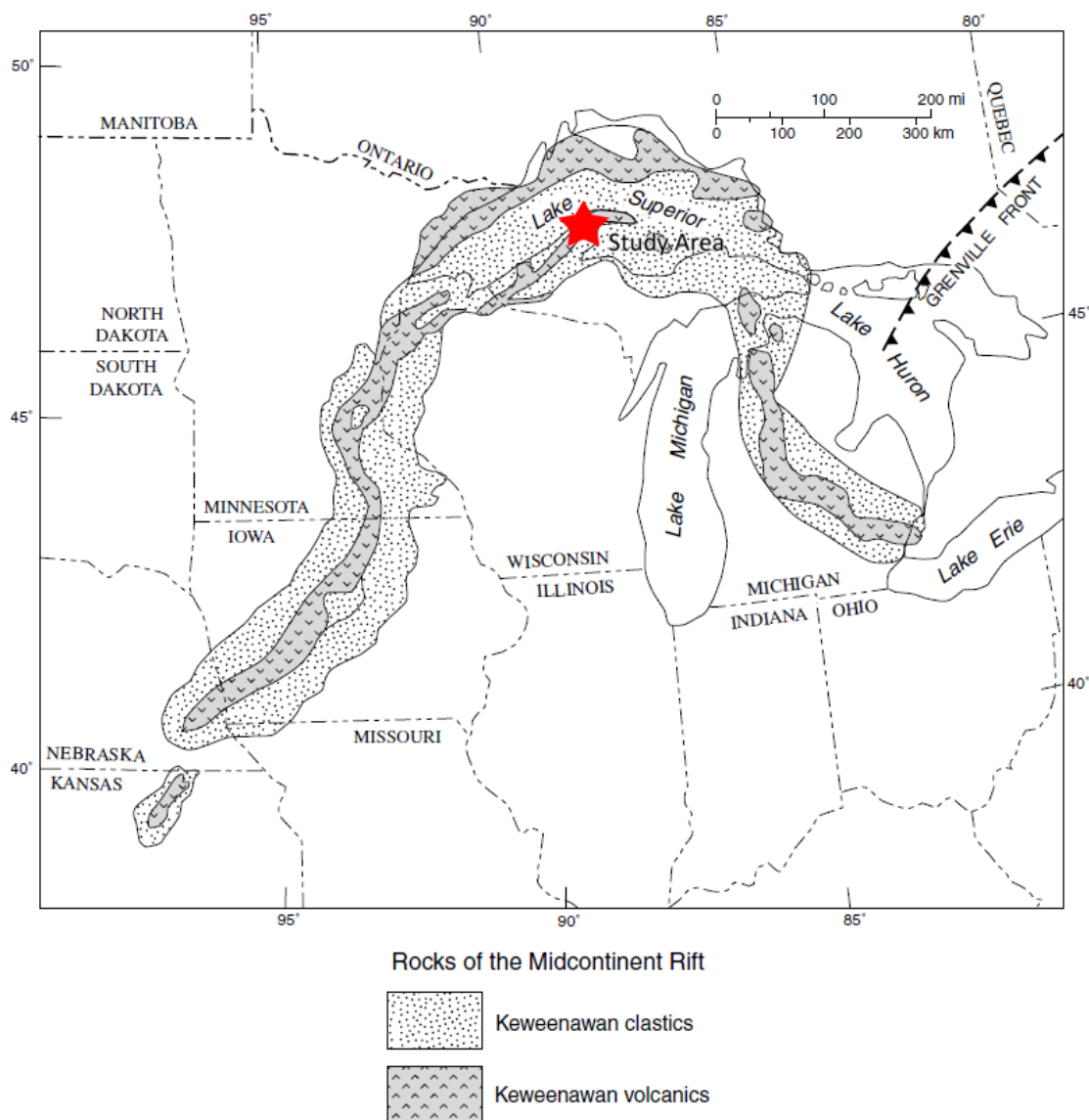
Figure 2: A map of the Midcontinental Rift system. The red star indicates the study area. Modified from Palacas et al. (1990) by Ojakangas et al. (2001).

The PLV sequence is a 10km thick package of over 200 basalt flows interbedded with conglomerates and sandstones. The flows are typically 10m thick, with a range in total thickness from 1 to 450m. They have a massive interior with vesicular or brecciated flow tops. Rhyolite lava flows account for less than 1% of the formation and are found only in the lower 0.5km of the PLV. The interbedded conglomerates and sandstones account for less than 5% of the exposed PLV and are typically red-coloured. The larger clasts of the PLV (pebble to boulder sized) are dominantly rhyolite, with some basalt clasts

(Nicholson, 1992; Bornhorst & Mathur, 2017). The PLV is overlain by the Oronto group; a series of sedimentary units ranging from red-colored conglomerates to grey-black shale and siltstones (Bornhorst & Mathur, 2017).

A metamorphogenic model for the deposition of copper is provided by Bornhorst and Mathur (2017) using $\delta^{65}Cu$ isotopic data to put constraints on the genetic model. The model describes the copper as having been leached from rift-filling basalts by deep low-sulfur metamorphic hydrothermal fluids, moving up-dip and precipitating copper upon mixing with meteoric waters (Brown, 2006) and undergoing water-rock reactions (Figure 3) (Bornhorst & Mathur, 2017).
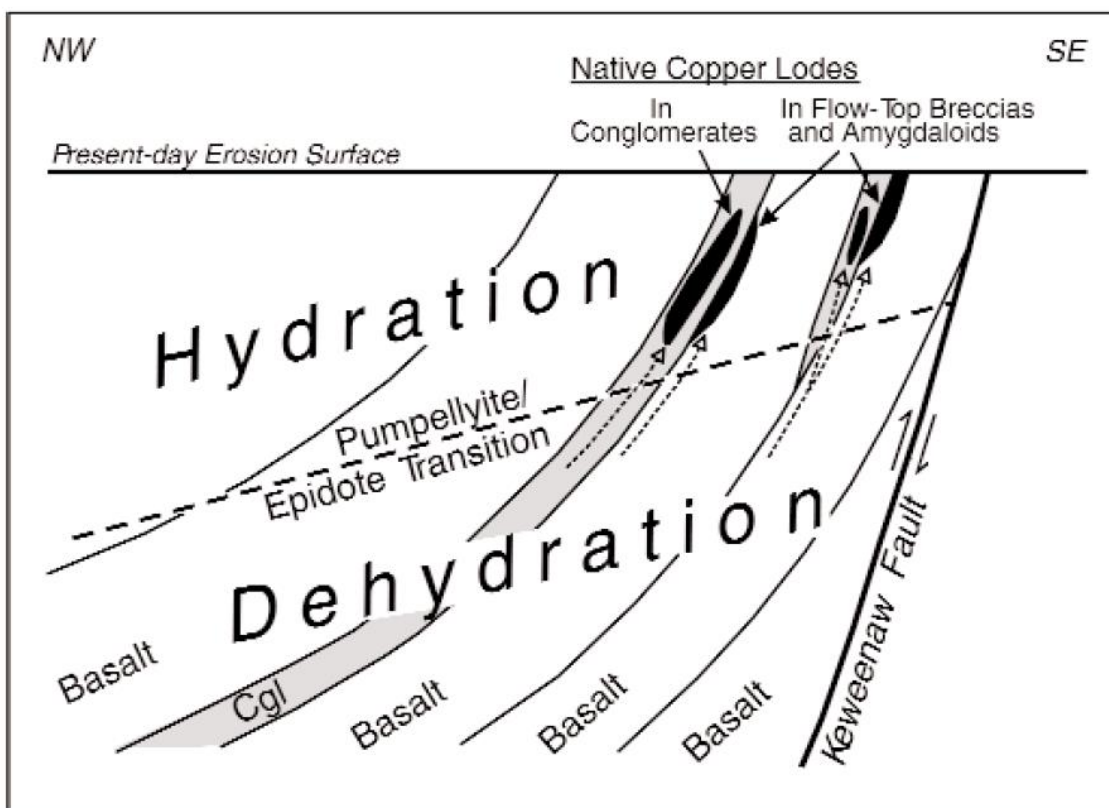
Figure 3: Schematic diagram showing the movement of ore-bearing fluids through the PLV. Metamorphogenic ore fluids are formed at depth below the copper deposits from the same basalt-dominated section which host the deposits. Dotted arrows show the movement of fluids up-dip through permeable flow-top breccia, amygdaloidal basalt, and conglomerate units. From Brown (2006).

1.3   Economic Background

Copper mining by Indigenous communities in the Keweenaw region may have begun as early as 7000 years ago, with a period of relative greater activity from 6000 to 3000 years ago (Bebber et al., 2019). Objects made from Keweenawan copper have been found in archeological sites across the North American continent (National Park Service, 2022c). Interest in the Keweenaw region for copper mining by European settlers saw an increase after Dr. Douglass Houghton visited in 1830, publishing a report 11 years later in 1841. The Pittsburgh & Boston Mining Co. were the first to open a successful mine in the region in 1845, the Cliff mine. Copper mining grew immensely throughout the region up until the first world war, after which there was a decline in mining activities (Butler & Burbank, 1929). Copper mining continued through the 1900's, with the oldest remaining mine closing down in 1968. Between 1845-1968, an estimated 10.5 billion pounds of copper was produced in the region from dozens of mines along the Peninsula. The final industrial mine, the White Pine mine, closed in 1997 (National Park Service, 2022b).

1.3.1   Ojibway Mine

The Ojibway Mine is situated in the Kearsarge Amygdaloid (Nicholson, 1995) of the PLV. An amygdaloid is a secondary deposit of minerals formed from cavities within volcanic rocks created by trapped gasses at the time of formation. The Ojibway mine was an underground operation which produced approximately 50,000 pounds of copper. Exploration on the site began in 1902 with the Ojibway Mining Company opening in 1907, producing copper for only six years before closing in 1913. Minerals found at this mine include copper, quartz, calcite, epidote, malachite, prehnite, and silver (mindat.org, 2022a). It was located on the northeastern end of the Kearsarge amygdaloidal lode, part of the Portage Lake Volcanics, in Keweenaw County (Figure 4). Copper mineralization from the amygdaloid units that were mined in the Keweenaw Peninsula were referred to as lodes.
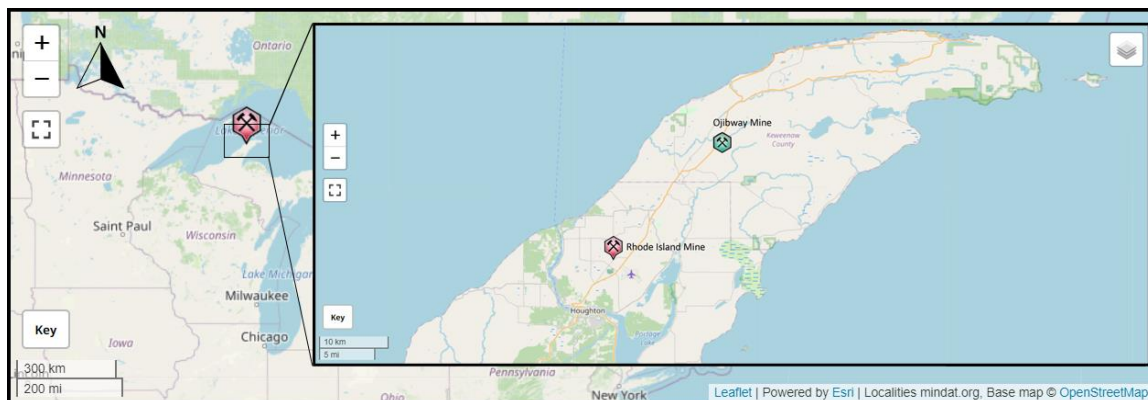
Figure 4: Map showing the location of the Ojibway mine (green icon) and the Rhode Island mine (red icon). Modified from mindat.org (2022a, 2022b).

The Kearsarge Amygdaloid was the most productive copper-bearing lode in the Keweenaw region (Nicholson, 1995), however, the two mineshafts sunk by the company were unproductive (Rosemeyer, 1998). Two basal flows were reported by the company; a flow at the No. 1 shaft was reported at 35-85 feet, and a flow at the No. 2 shaft was reported at 260-350 feet (Butler & Burbank, 1929). Areas with high quartz content within the amygdaloid were found to correlate with rocks with little copper, something which was evidenced by the rock dumps from this mine (Stoiber & Davidson, 1959).

1.3.2   Rhode Island Mine

The Rhode Island mine consisted of three mineshafts, targeting the Allouez conglomerate and the Pewabic amygdaloidal lode (Figure 4). Mining originally started in 1860 and closed 5 years later in 1865 due to a lack of returns, however the mine reopened in 1899 and continued until closing once more in 1906. When the mine reopened a third time in 1910 under new management of the Franklin Mining Company, they dug a new shaft into the more economically viable Pewabic lode, working intermittently until finally permanently closing in 1920. Minerals reported from this mine include copper, epidote, quartz, prehnite, and calcite (mindat.org, 2022b).

The Allouez conglomerate which was first mined is characterized by its red sedimentary units consisting largely of conglomerates, with some sandstone and siltstone. It's interpreted to be from a terrestrial alluvial fan deposit and was deposited between

amygdaloidal basalt flows, with boulders larger than 20cm consisting of mafic rock, quartz porphyry, and granophyre clasts (Bornhorst & Rose, 1994; Nicholson, 1997).

The Pewabic lode is made of thin brown to brownish-green andesitic amygdaloidal lava flows (Butler & Burbank, 1929). Large feldspar phenocrysts were often reported, with interconnected vesicles creating channels for the eventual flow of hydrothermal ore solutions (Rosemeyer, 2010).

1.4   Cultural Significance

On discussion of copper in the Keweenaw region, it is important to acknowledge and understand the historical and cultural importance of copper to the Native American peoples that have lived in the region for generations. Redix (2017) expresses how important copper was, and continues to be, to the Native American communities of the Keweenaw peninsula. The removal and mining of these natural copper resources was a direct act of colonialism in the region, with mineral exploitation rights only being achieved through misrepresenting treaties that the Ojibwe in the region had signed.

As we look to the Keweenaw region for the purpose of this research, we must also be prepared to acknowledge the impacts of colonialism on the history of economic geology. The cultural and spiritual appropriation of important artifacts is something that must be understood, as well as the physical impacts that mining has had on the communities in the Keweenaw Peninsula.

Due to the purity of Keweenawan copper, little to no chemical processing was required. However, mine wastes still exist in the forms of waste rock piles, tailings from stamp mills (stamp sands), and slag from smelters (Gohman, 2013). Waste rock piles have largely diminished after being reclaimed for use as construction materials, however the stamp sands and slag were most often dumped into waterways, with stamp sands posing the greatest environmental risk (National Park Service, 2022a). In a solid phase, copper is not particularly harmful. However, mobilization of copper from these stamp sands into surface waters results in a series of oxidation reactions from solid copper to cuprite, and then further oxidation yields dissolved Cu and malachite (Jeong et al., 1999). These high

concentrations of copper can adversely affect aquatic food webs, with concentrations of the trace metals aluminum, barium, chromium, iron, manganese, nickel, vanadium, and silver identified as exceeding Ecological Risk Screening Levels for Aquatic Life (ERSL) in the Keweenaw Bay. Pollution such as this that impacts Lake Superior and the fish that live in it infringes on Ojibwe treaty rights to harvest natural resources from the lake (Kerfoot et al., 2020).

One notable example of the impacts of colonialism is the Smithsonian's denial of the Keweenaw Bay Indian Community's (KBIC) request to return the Ontanagon boulder, a 3000 pound copper boulder which was removed from Michigan in 1843. In his 2017 paper, Redix presents a clear argument for the cultural importance of the copper, and why the boulder should be repatriated. Linguistic evidence and historical records show that the boulder was clearly viewed as a being, referred to as "our hope and our protection" by people at the time.

We believe that it is important to understand and respect the cultural importance and history of the copper that we are researching, so that the materials may be handled as respectfully as possible. It is for this reason that we began looking to use non-destructive micro-computed X-ray tomography (microCT) scanning to examine our samples, alongside SEM analysis. In doing so we aim to minimize the impact our research will have on these samples, and we will be able to explore new investigative methods in the process.

Chapter 2

2 Methods

A summary of the materials and methods used in this study is presented here. Sample preparation procedure is described following sample K-21-4A, the first to be prepared for analysis in this project. Results of this analysis are presented below in chapter 3.

2.1 Previous Works

Similar work regarding the combination of microCT and SEM analysis has been done on meteorites by Zhang et al. (2021), using both techniques to identify inclusions and investigate pore and fracture networks throughout their samples. However, they mounted their samples for SEM analysis after having done their microCT work. Chisambi et al. (2020) explored combining both methodologies with gold deposits, analyzing drill core samples for gold and noting the effectiveness of combining these methodologies.

Currently we know of no integrated scanning electron microscope energy dispersive X-ray spectroscopy (SEM-EDS) and electron backscatter diffraction (EBSD) analysis work done to analyze the strain history of the copper from the Keweenaw Peninsula.

2.2 Materials

The study area was inaccessible due to Covid, so exploratory work began on a suite of samples donated to Western University from the collection of Mr. Arnim Walter. These were labeled by mine site and had no information on the history of treatment of the samples. It is assumed that, as with most copper collected by mineral enthusiasts, the vein samples have been exposed to acid etching to remove matrix minerals. Other samples such as the pore-filling specimens were likely collected from mine dumps and were therefore processed by mining equipment (blasting, crushing). The samples selected for analysis are of the vein, amygdule, and sedimentary types, and are from the Rhode Island and Ojibway mines. They have the sample numbers K-21-4A (Ojibway mine), K-21-2 (Rhode Island mine) and K-21-7 (Rhode Island mine). Optical and SEM methods were used to characterize the copper and surrounding minerals. The EBSD technique in

particular has not been previously applied to Keweenawan copper samples to the best of our knowledge (T. Bornhorst, pers. Comm. 2022).

2.3   Methods

The workflow developed for these samples began with optical characterization using conventional techniques and progressed to several microscopy techniques; the scanning electron microscopy (SEM) techniques Energy Dispersive X-Ray Spectroscopy (SEM-EDS) and Electron Backscatter Diffraction (SEM-EBSD), and micro-computed X-ray tomography (microCT). These results are presented in Chapter 3. SEM sample selection began with a visual examination of multiple samples from those donated to Western University. Sample K-21-4A was chosen as the sample for this experiment as a representative sample of a vein-type copper deposit with minimal alteration. The sample was cut with a Buehler slow speed saw down to a section less than 2 cm thick. The sample was given a physical polish to create a perfectly flat surface before being set into a 1¼ inch epoxy plug.

The sample then underwent a sequence of conventional and specialized polishing steps. This began with a physical polish at the Western University thin section lab beginning with silicon carbide paper on a tabletop lapping wheel. They were then polished with 3µm and 0.25µm diamond powders in oil on Strueters RotoPol 35 machines. Then a vibratory polish was applied using the Vibromet vibratory polisher, and polishing was finishing with an ion polish using the Hitachi 4000 Argon Ion Mill at the ZAPlab to prepare it for SEM-EDS and SEM-EBSD analysis (Figure 5). The sample underwent carbon coating at Surface Science Western as well as optical microscope mapping. This imaging is done with the Keyence VHX-6000 digital microscope by joining multiple smaller pictures taken at a higher zoom setting and stitching them together to create a single continuous optical or reflected light map of the full surface (Figure 7). Samples were then sufficiently prepared to be examined with a full suite of instrumentation, with the success of these methods detailed in Table 1.

Figure 5: A) Vibromet Vibratory polisher. B) Hitachi 4000 Argon Ion Mill. C) The Hitachi SU6600 variable pressure Field Emission Gun Scanning Electron Microscope. Arrows indicate the attached energy dispersive X-ray detector and electron backscatter diffraction detector. D) The interior of the Zeiss Xradia 410 Versa from Surface Science Western. Arrows indicate the X-ray emitter, the sample in the sample holder, and the X-ray collector.

Table 1: Sample number (left column) and corresponding type(s) of analysis (see text for unabbreviated terms). Y signifies work completed, NA indicates that the technique was not applied to the sample, and X signifies technique was unsuccessful.

	SEM-EDS	SEM-EBSD	MicroCT
K-21-2	Y	Y	NA
K-21-4A	Y	X	Y
K-21-7	Y	Y	NA

2.3.1   SEM-EDS

The optical, stitched image was imported to the Hitachi SEM software registered with SEM stage coordinates for navigation and recording analysis locations. Once the sample was loaded into the SEM, image registration is done through the AZtec software from Oxford Instruments.

To register an image, the SEM field of view is moved to a readily identifiable point (e.g. an edge) of your sample surface. The same point on the imported optical image that you have loaded into the AZtec software is double clicked to register a point. Next, you move to an identifiable point on the opposite side of the sample and repeat this process. Selecting points that are diagonally across from each other is ideal, as it will ensure the movement of the stage within the sample chamber is accurate in both the X and Y directions. Registration was done to improve efficiency in moving the sample in the SEM chamber, and to provide ease of use to find and relocate regions of interest on the sample. Once image registration has been completed properly, you are able to double click on the image withing the AZtec software and it will automatically move the sample in the SEM chamber to the point highlighted.

A Hitachi SU6600 variable pressure Field Emission Gun Scanning Electron Microscope (FE SEM) at the Western University ZAPLab was used for SEM-EDS elemental analysis. SEM-EDS automated surface mapping was set up through the AZtec software. SEM-EDS analysis is taken for multiple individual fields covering the sample surface, which are then stitched together within the software to create an SEM-EDS map of the entire surface.

Initial SEM-EDS mapping was done over a small region of the sample to determine an ideal balance between resolution and scan time (Figure 6). A value of 10 frames per field of view area was selected for a full-surface stitched montage, giving enough resolution to identify micrometre-scale features such as the small domain of silver seen in Figure 6B, without extending the scan time.
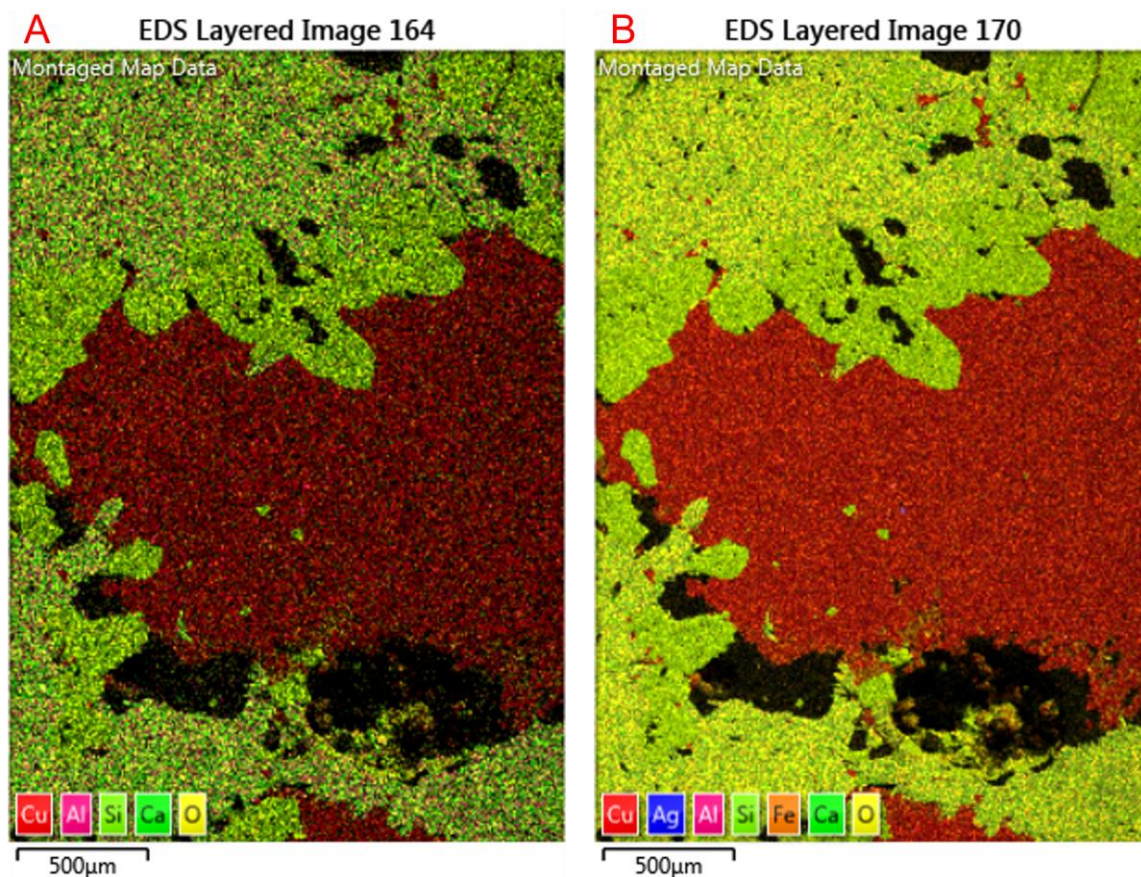
Figure 6: Energy dispersive X-ray spectroscopy mapping frame count image comparisons. The 1 frame stitch (A) has notably lower contrast than the 10-frame stitch (B). The 10-frame stitch also was able to identify additional elements not seen in the shorter scan, including silver and iron.

2.3.2   SEM-EBSD

The Hitachi SU6600 SEM was used for the EBSD analysis equipped with an Oxford Instruments Symmetry camera (Figure 5). Samples were mounted at a 70° angle to the incident (vertical) electron beam and loaded into the chamber, where the attached EBSD

detector is then inserted. EBSD mapping was controlled by Oxford's AZtec software. Postprocessing of EBSD maps was done using the Channel5 software. The "wild spikes: extrapolate" post-processing function was applied after importing into the Channel5 HKL Tango software to find and replace "lonelies" within the data, which are isolated measurements with misindexing. The AZtec software and SEM-EDS allowed for the use of the TruMap function, which records SEM-EDS and SEM-EBSD data for each pixel on the map. By combining both crystallographic and elemental data, phase identification within each map is possible.

2.3.3   Micro-computed X-Ray Tomography

MicroCT analysis was carried out with a Zeiss Xradia 410 Versa at Surface Science Western. The sample was oriented with a thin strip of copper tape and mounted to a stand to be placed within the machine. Scans with no filter were ran at 80Kv, and the BR6 scan was run at 140Kv. Completed scans were reconstructed and imported to the ORS Dragonfly software for analysis. To stitch the two air scans together, the "normalize histogram" function was run, with the original vertically oriented scan chosen as the reference point to normalize against. Then the "stitch 3D datasets" function was employed, using both mean and weighted sampling methods to compare efficiency.

Chapter 3

3 Results

Three samples were investigated in detail with a suite of instrumentation, and the results are presented below according to the measurement technique. Optical, SEM imaging, and chemical measurements are presented first for all three samples (K-21-4A. K-21-2, and K-21–7), followed by SEM-EBSD of the latter two samples. MicroCT results are then presented for one of these samples (K-21-4A). A synthesis and interpretation of what these observations can tell us about the crystallization and deformation history of Keweenawan copper in each sample, and then the success of the analytical techniques used, are presented consecutively in Section 4 (Discussion).

3.1 Characterization by Optical AND SEM-Energy Dispersive Spectroscopy (SEM-EDS)

Following optical inspection and imaging, all samples were then fully surface mapped using SEM-EDS at the Western University ZAPlab. Regions of interest (ROI) were investigated in greater detail with SEM-EDS mapping and point and ID, which are also presented here.

3.1.1 Sample K-21-4A; Vein-hosted Copper

Sample K-21-4A is a 1.5cm by 2.5cm light-coloured sample from the Ojibway mine site. Based on sample mineralogy it is presumed to be from a vein-type copper occurrence, with the main mineral consisting of a pale white, seemingly massive mineral within which blebs and narrow stringers of copper are distributed randomly (Figure 7).
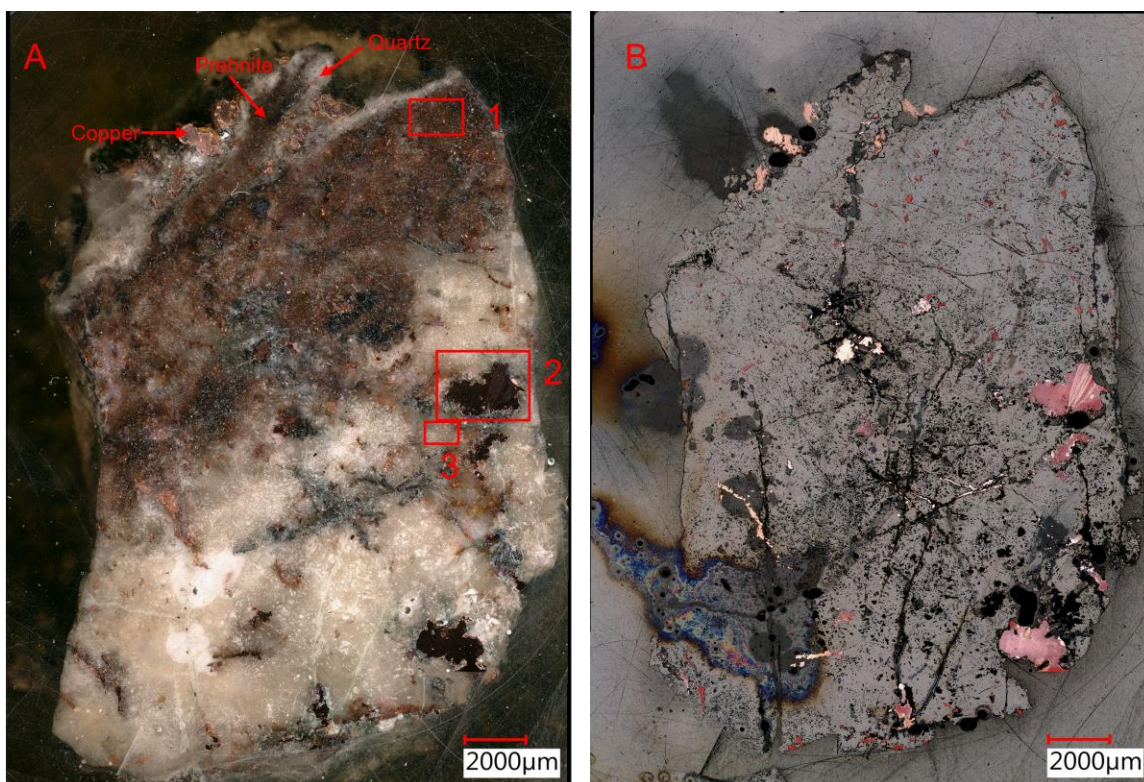
Figure 7: Stitched visible and reflected light images of a polished surface of the sample cast in epoxy, taken with ring (A) and coaxial (B) lighting, respectively. Regions of interest where more detailed scanning electron microscopy work was performed are annotated as red boxes in (A), which link to other Figures in this section.

The SEM-EDS mapping and point analyses indicate that the sample consists mostly of three minerals: a white Ca-Al silicate, quartz, and copper (Figure 8). Point analyses of the Ca-Al silicate yield these elements and proportions in weight % based on X-ray energy intensities: O (60%), Si (17%), Ca (10%), Al (10%), Fe (1-3%). The appearance and compositional abundances together suggest that this mineral is prehnite ($Ca_2Al_2Si_3O_{10}(OH)_2$). The prehnite texture is one of interlocking, randomly oriented, 100µm –wide blades (Figure 9), with some small interstitial pore spaces.
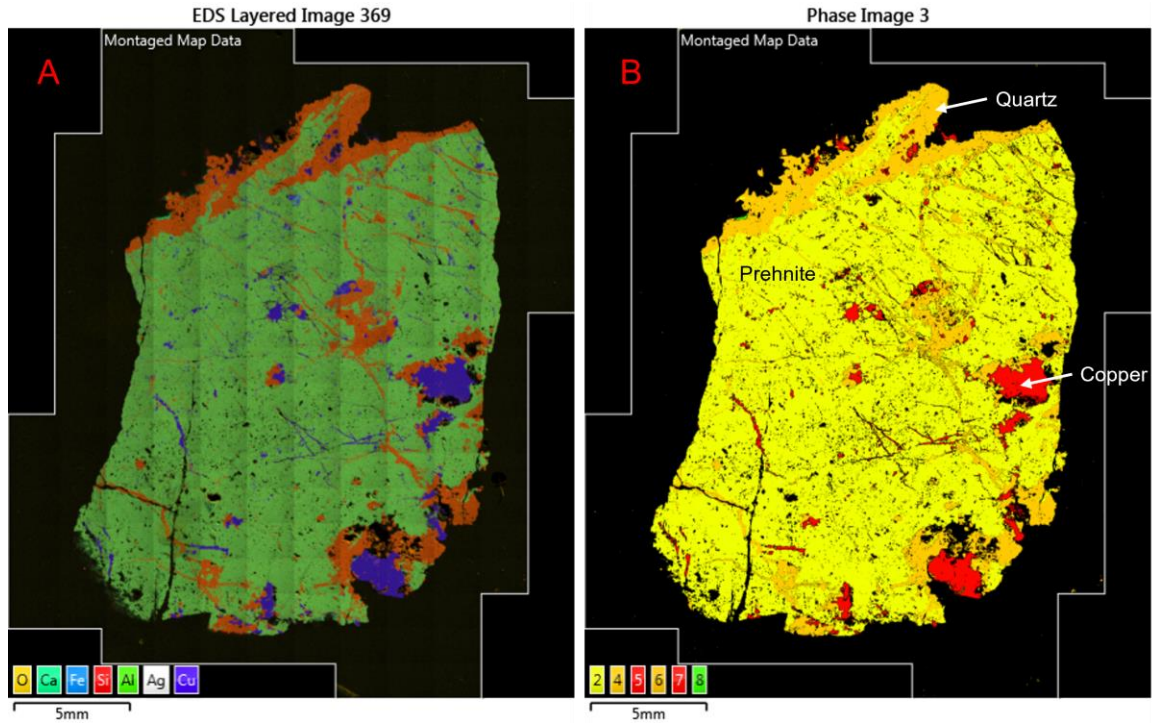
Figure 8: Energy dispersive X-ray spectroscopy mapping (A) and Aztec phase mapping (B) results for sample K-21-4A. In (B), the three main rock-forming minerals are: Ca-Al silicate (likely prehnite, yellow), quartz (deep yellow) mostly as veins, and copper (red) with quartz and as large, sub-cm blebs.

Copper occurs mainly in two forms: as larger blebs up to ~2mm across, and as smaller disseminated domains (100-200μm in width) sometimes in the interstices of prehnite blades (Figure 9) and other times as partly infilling veins in association with quartz (Figure 10). There is no evidence of alteration minerals in these microscopic domains. Within one of the large blebs of copper a small inclusion of μm-scale silver was also identified (Figure 11). The quartz and copper appear late in the crystallization sequence, forming after the matrix prehnite.
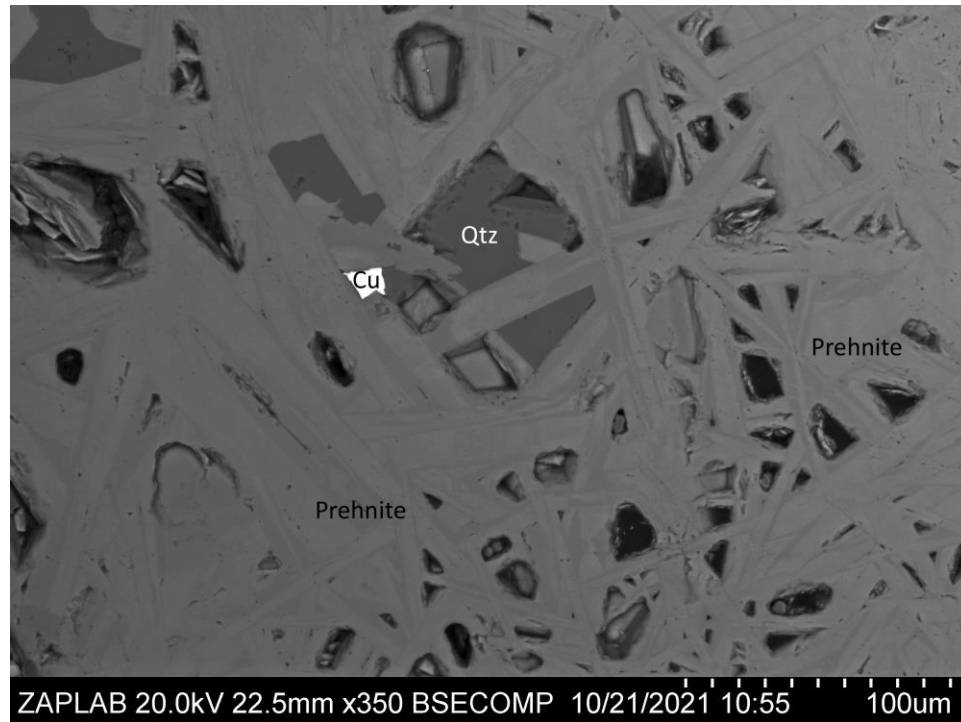
Figure 9: Backscatter electron image of K-21-4A at region of interest #3 showing the 100µm scale interlocking blades of the main mineral (likely prehnite). Slight variations in trace amounts of iron (1-3%) create the slight differences in grey, the lighter grey containing ~2-3% iron and the darker grey >1%. Copper (bright) can be seen in interstices of prehnite blades.
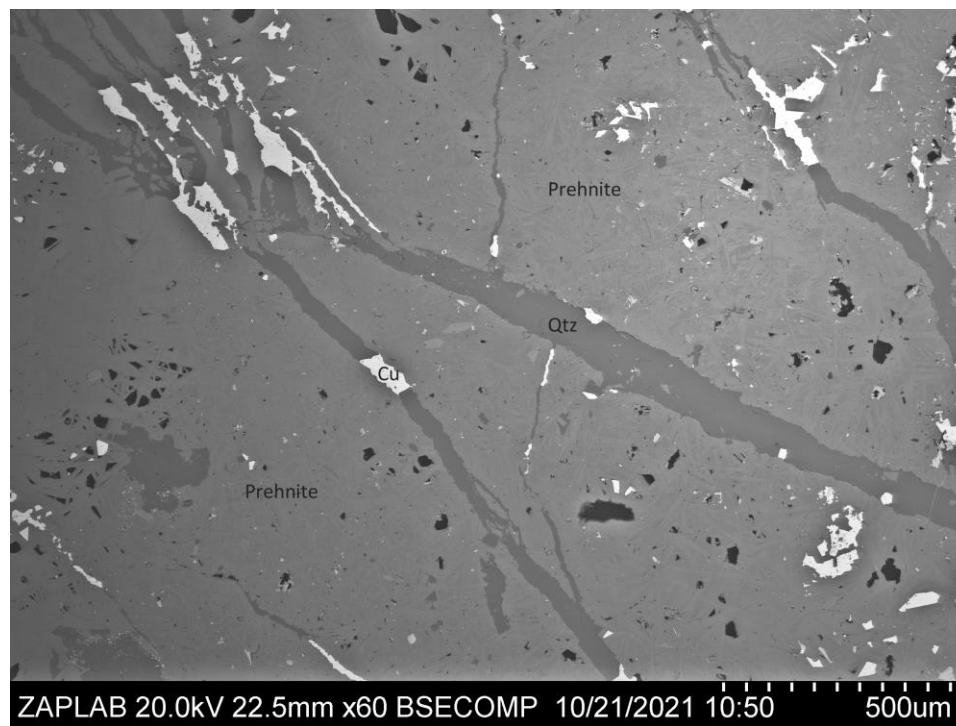
Figure 10: Backscatter electron image of K-21-4A at region of interest #1 showing fine quartz veins (dark grey) with copper (bright) as disseminated 100 to 200µm domains free of alteration.
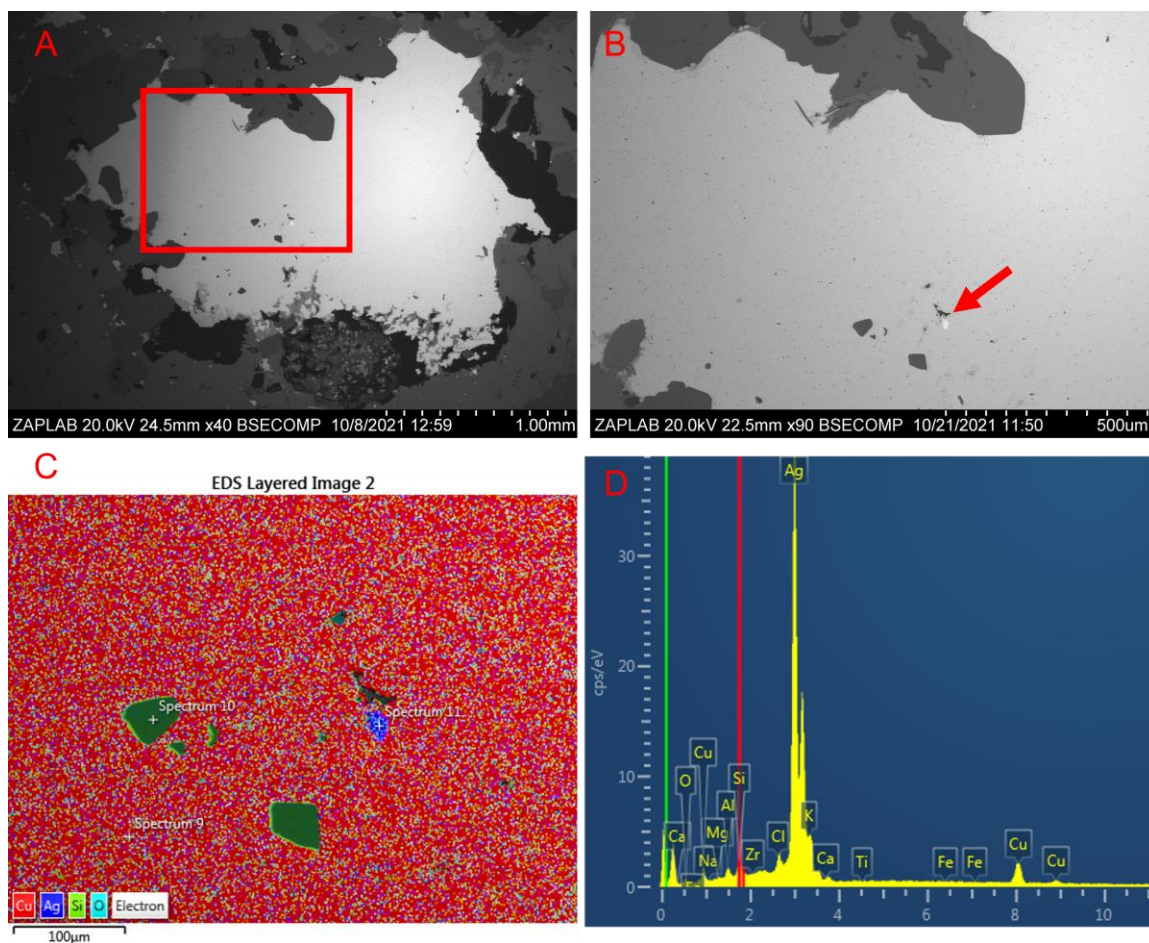
Figure 11: A) Backscatter electron image of a relatively large copper domain within the sample. B) higher magnification backscatter electron image of the copper domain with arrow indicating an inclusion of silver. Note euhedral quartz crystals within the copper. C) Energy dispersive X-ray spectroscopy map of the silver inclusion from (B), spectrum 11 is shown in (D) to be silver. The dark green minerals (Spectrum 10, C) are small (10-50μm) quartz grains.

3.1.2   Sample K-21-2; Sediment-hosted Copper

Sample K-21-2 is composed mostly of fine-grained sedimentary rock (siltstone) from the Rhode Island Mine. It is reddish in appearance and exhibits copper on one edge in a small vein associated with quartz and epidote. The sample was sawn at a right angle to the plane of the vein. The two sample halves were then lain on double-sided tape and cast as 2cm by 1cm slabs in an epoxy plug (Figure 12A).
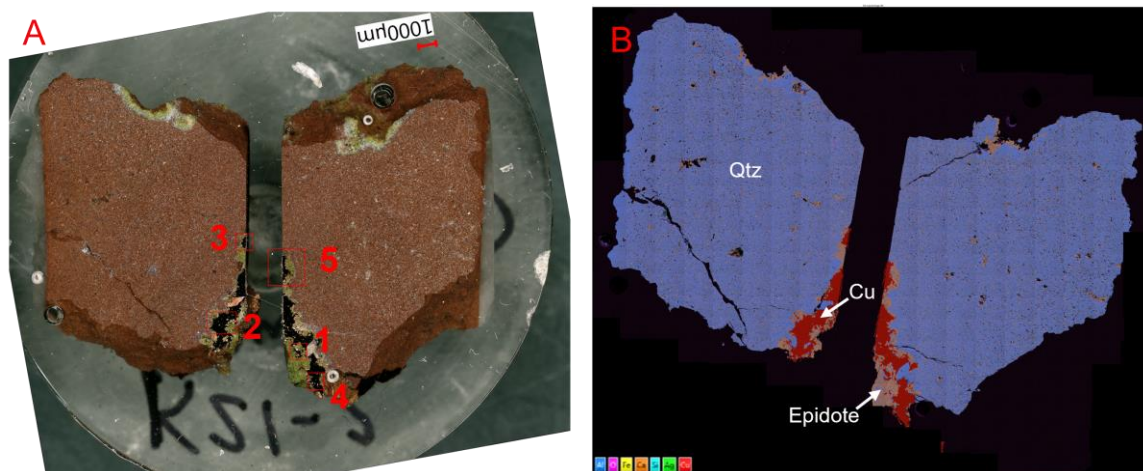
Figure 12: Optical image (A) and energy dispersive X-ray spectroscopy map (B) of two halves of sedimentary sample K-21-2 hosting a small vein of copper in association with quartz and epidote. Regions of interest where more detailed scanning electron microscopy work was performed are annotated as red boxes in (A), some of which link to other figures in this section.

SEM-EDS mapping and point and ID indicate that the sample consists primarily of 10μm quartz grains, many of which are iron-stained. Iron oxide grains were also identified within the quartz grain matrix. The copper in the vein is associated with a green Ca-Al-Fe phase not found in the main siltstone body of the sample (Figure 12B). Point analyses on the Ca-Al-Fe phase by Buyers (2022, B.Sc. thesis) gave a rough average elemental composition in weight % of O (40%), Si (19%), Ca (16%), Al (13%), and Fe (12%). The visual properties and elemental abundances of this mineral are consistent with the common mineral epidote; $\{Ca_2\}\{Al_2Fe^{3+}\}(Si_2O_7)(SiO_4)O(OH)$. The epidote forms subhedral grains, of 50-200μm average diameter, intergrown with subhedral to euhedral quartz grains (100-500μm diameter) (Figure 13). The copper occurs as large (1-3mm) subhedral domains infilling space between euhedral quartz and epidote (Figure 13). SEM-EDS mapping indicates that the host siltstone is enriched with in silica within 500μm of the vein.
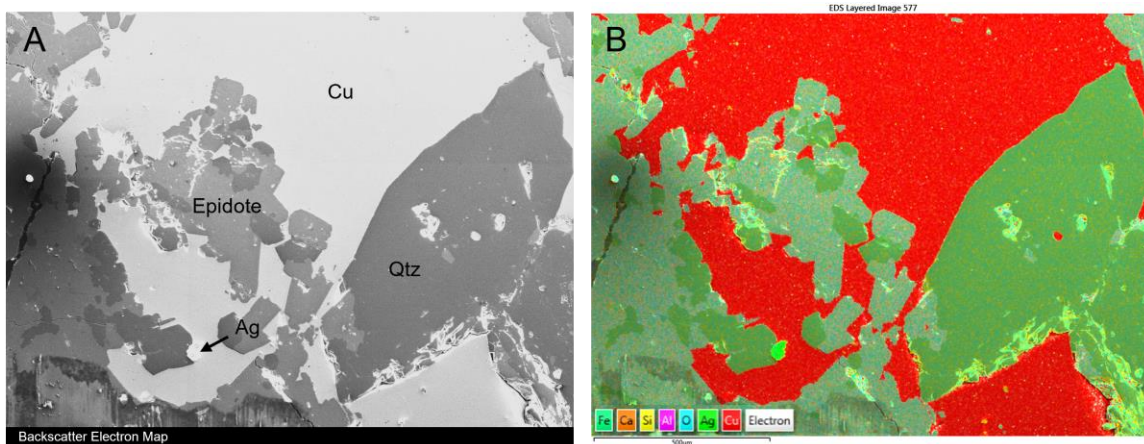
Figure 13: Backscatter electron (A) and energy dispersive X-ray spectroscopy (B) images showing the texture of the copper, quartz, and epidote in sample K-21-2, region of interest #1 in Figure 7A. One small bleb of silver (bright green, (B)) was also identified.

3.1.3   Sample K-21-7; Amygdule-hosted Copper

The roughly hemispherical sample K-21-7 had been cut and polished prior to this study, presumably by the collector. It is a ~2cm diameter, dark-coloured sample from the Rhode Island mine. On the cut face it features orange and grey domains surrounding a core zone rich in natural copper (Figure 14A). Based on sample mineralogy and location it is believed to be from an amygdular basalt unit at that mine site. Reflected light microscopy of the large central copper domain revealed a small domain of what was later confirmed to be natural silver. The sample was cut again to form a thin (.5cm) slab and cast in a 1" diameter epoxy plug.
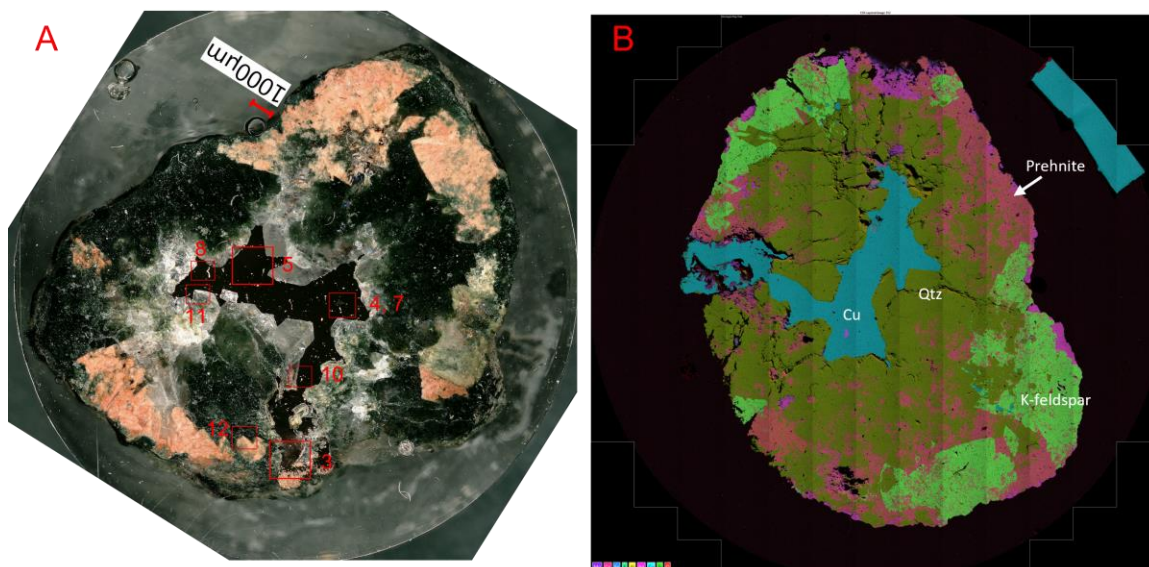
Figure 14: Optical (A) and energy dispersive X-ray spectroscopy (B) maps of sample K-21-7. Red boxes indicate regions of interest within the sample which were targeted for energy dispersive X-ray spectroscopy and electron backscatter diffraction analysis.

SEM-EDS mapping and point analyses indicate that the four main minerals show a broadly concentric zonation consisting, from rim to core, of Al-Ca-Fe silicate, a K-bearing silicate, as well as quartz and copper. A fifth Fe-Mg bearing mineral close to the rim has not yet been identified (Figure 14B). The pink K-bearing phase yielded elemental (and X-ray intensity) point analysis values in weight % of O (40%), Si (33%), K (15%), Al (10%), and based off that data and visual physical properties it is likely potassium feldspar ($KAlSi_3O_8$). The green, Al-Ca-Fe mineral has a composition of O (41%), Si (20%), Ca (17%), Al (12%), Fe (8%), Mg (2%), and together with its visual properties, is taken to be epidote ($\{Ca_2\}\{Al_2Fe^{3+}\}(Si_2O_7)(SiO_4)O(OH)$). The unidentified Fe-Mg mineral phase has an average composition of O (40%), Si (18%), Mg (16%), Fe (15%), Al (11%).

The sample consists primarily of euhedral quartz and potassium feldspar, with epidote alteration visible in association with the feldspar (Figure 15). Epidote "finger" texture could be seen within the quartz and copper with visual microscopy (Figure 16). Copper occurs primarily as one large bleb through the center of the sample, infilling a pore space

between the euhedral quartz crystals. This copper domain also was found to have a ~.5mm natural silver domain near the central region (Figure 17).
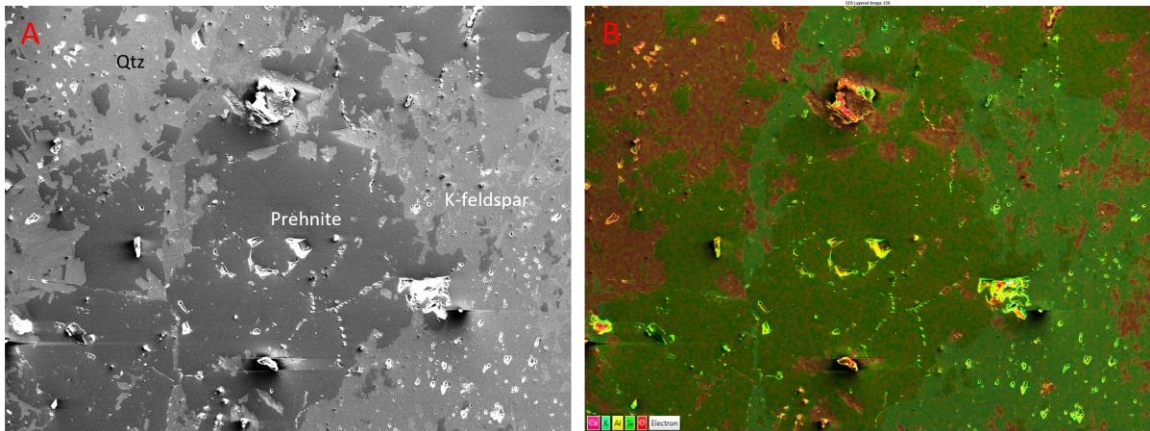
Figure 15: Backscatter electron (A) and energy dispersive X-ray spectroscopy (B) maps showing intergrown textures of quartz (light grey), potassium feldspar (medium grey), and prehnite (dark grey) from region of interest #12.
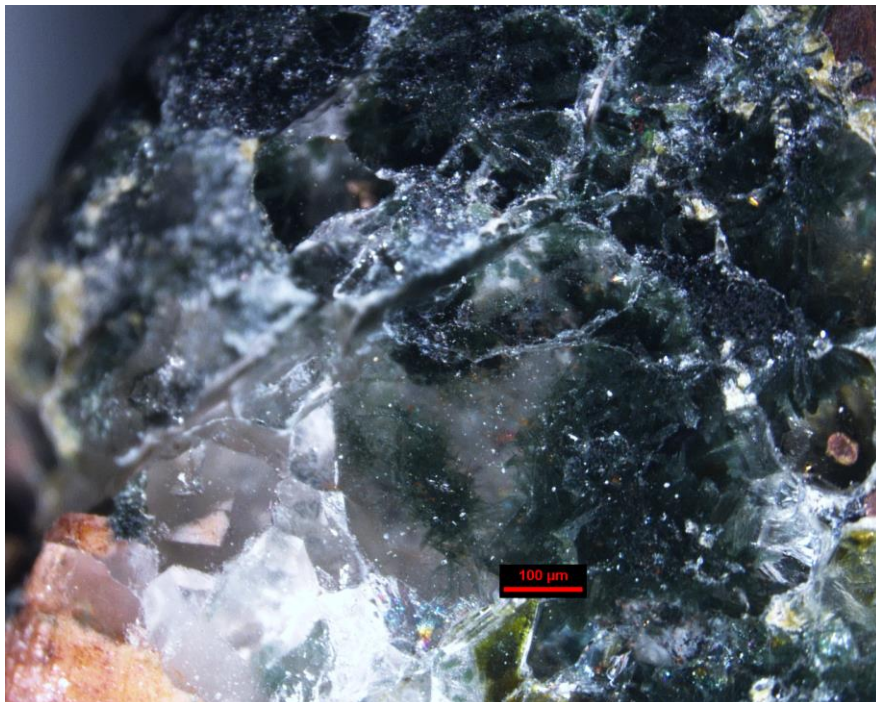
Figure 16: Optical light image showing the epidote "finger" texture growing into quartz.
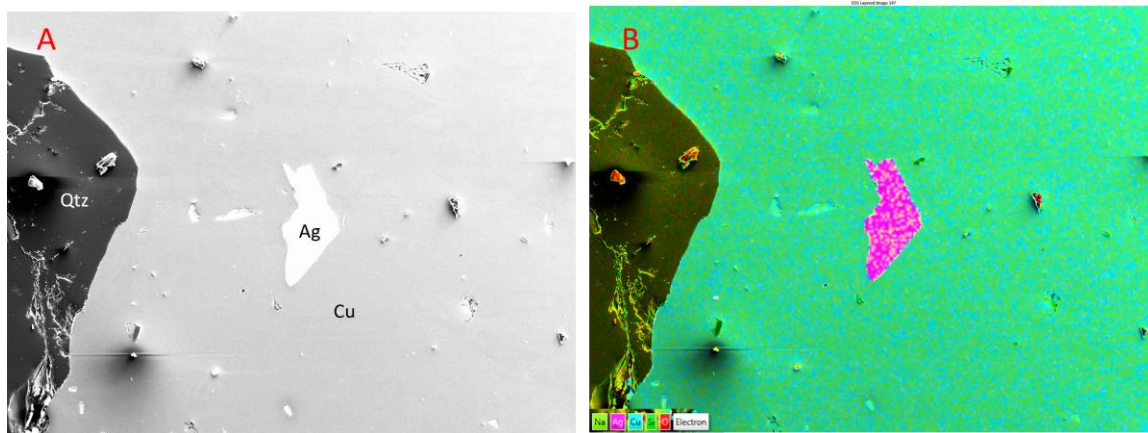
Figure 17: Backscatter electron (A) and energy dispersive X-ray spectroscopy (B) maps of region of interest #4 in Figure 14A showing a subhedral domain of natural silver within copper.

3.2 SEM-Electron Backscatter Diffraction (SEM-EBSD)

Two of the three samples were successfully analysed with the SEM-EBSD technique. The results are presented for each sample under these categories; data quality (including reference to a table of SEM-EBSD run conditions) and phase identification followed by texture and microstructure. Due to its high spatial resolution and sample geometry, SEM-EBSD maps are generally performed at high magnification. For each sample a detailed map is referred to as a ROI. In Chapter 4, these SEM-EBSD results will be interpreted together with the SEM-EDS data.

3.2.1 Sample K-21-2; Sediment-hosted copper

SEM-EBSD mapping was carried out at ROI #5 (Fig 12A,) where the map boundaries cover the saw-cut sample contact with epoxy mounting material.

3.2.1.1 Data Quality and Phase Identification

The SEM-EBSD analysis at this site lasted for a total run time of 3:59:17. Zero solutions accounted for 60.97% of pixels, however this scan was run on the edge of the sample and included the amorphous epoxy (39.03% of the zero-solutions). Two phases were identified: quartz and copper. The Electron Backscatter Patterns (EBSP's) of copper had

higher band contrast than quartz (Figure 18A) leading to lower Mean Angular Deviation values relative to the reference diffraction pattern (Table 2).

Table 2: Data summary for SEM-EBSD mapping of sample K-21-2, ROI #5.

Phase	Step Size (µm)	Indexed pixels (%)	Mean BC (min/max)	Mean MAD (min/max)
Zero Solutions	1.138	60.97	61.0	n/a
Copper	1.138	31.59	174 (30.0/227.0)	0.6573 (0.2156/1.9990)
Quartz	1.138	7.44	79.8 (30.0/115.0)	0.9971 (0.1828/1.9985)
Total	1.138	100.00	98.1	0.7221

3.2.1.2   Texture and Microstructure

The copper texture varies with distance from the plane of the saw cut. Away from the cut, the grain size is larger than the map area as no high angle (>10°) grain boundaries were observed. Interestingly, there is a small copper domain adjacent to quartz, seemingly isolated from the main copper domain, nevertheless the same crystal orientation (Fig 18B, C), suggesting crystallographic continuity across a large length scale. In detail, there is very minimal misorientation across the copper crystal (~3-5°) (Fig 18D). The texture changes markedly within 50 microns of the cut surface. In this tabular zone, the copper is fractured into parallel plates that are polycrystalline, with equant elongate grains having minimum dimensions of 10 µm. Intergrown with the edge of the copper vein are subhedral quartz grains of 10-100 µm size which were identified and do not appear to have a shape or crystallographic preferred orientation.
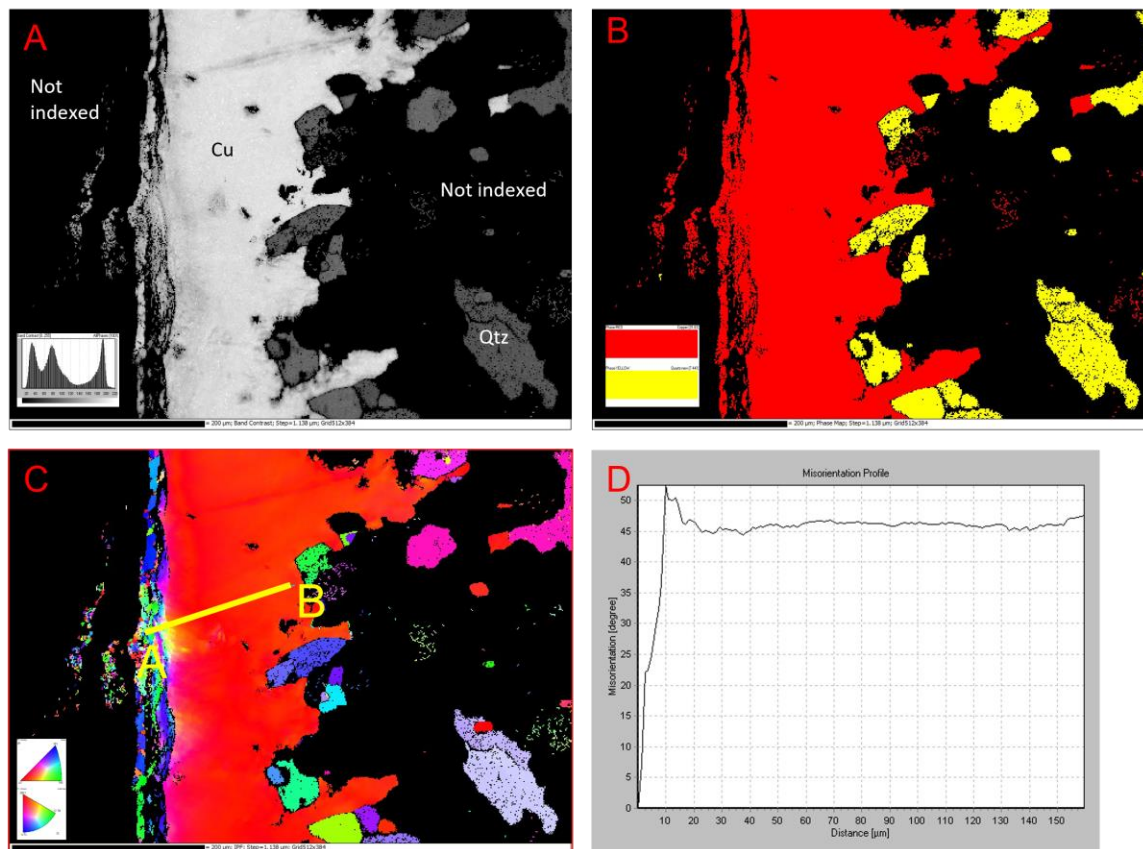
Figure 18: Map images of band contrast (A), phase maps (B), and inverse pole figure colouration (C) for sample K-21-2 at region of interest #5. D) Misorientation profile of section A-B in image (C).

3.2.2   Sample K-21-7; Amygdule-hosted copper, ROI #10

SEM-EBSD mapping was carried out at ROI #10, where the copper and quartz are in contact.

3.2.2.1   Data Quality and Phase Identification

The total run time for region of interest #10 (Fig. 14A, above) was 5:58:56. Zero solutions accounted for 14.7% of pixels, and 85.2% total of pixels were indexed. Again, there was higher band contrast from the copper EBSP's than from the quartz (Table 3).

Table 3: Data summary for SEM-EBSD mapping of sample K-21-7, ROI #10.

Phase	Step Size (µm)	Indexed pixels (%)	Mean BC (min/max)	Mean MAD (min/max)
Zero Solutions	2.782	14.74	68.7	n/a
Copper	2.782	41.21	119.3 (27.0/169.0)	0.8188 (0.1130/1.9999)
Quartz	2.782	44.05	80.85 (27.0/213.0)	1.045 (0.1429/1.9998)
Total	2.782	100.00	94.9	0.9358

3.2.2.2   Texture and Microstructure

The copper exhibits two styles of deformation throughout the sample, showing irregular patterns of internal deformation of up to 5° within single grains that are 100-300 µm in size. Twinning is seen within the copper somewhat frequently, with twins from ~200 µm long and ~10 µm wide. These copper twins are deformed by ~60° about the -111 axis compared to the main body of the copper (Figure 19C), and may show internal deformation along the same patterns as the rest of the copper grains. There is no difference in deformation pattern relating to proximity to the quartz grains seen also in this section, and it appears to have random preference.

Figure 19: Map images of band contrast (A), phase maps (B), and inverse pole figure colouration (C) for sample K-21-7 at region of interest #10. D) misorientation profile of section A-B in image (C). Black pixels in A, B, and C represent locations with zero solutions that were not indexed.

Large euhedral quartz grains are intergrown at the edge of the copper vein. The main grain is larger than the map area, however, there are smaller anhedral subdomains with a different orientation identified within the main quartz domains. These subdomains share a preferred orientation within the main quartz crystal, and all quartz crystals have minimal deformation (less than 2°) (Figure 19C).

3.2.3 Sample K-21-7; Amygdule-hosted copper, ROI #4

SEM-EBSD mapping was carried out at ROI #4, where a bleb of natural silver was identified within the copper.

3.2.3.1 Data Quality and Phase Identification

Two SEM-EBSD maps were run on this location, a first at smaller resolution with TruMap enabled to confirm the phases, and a second at higher resolution for greater detail.

The run time of the first map was 0:30:45. Zero solutions accounted for 16.96% of the sample, with 83.04% total pixels indexed. Silver and copper have the same unit cell structure (FCC), and as such, this scan was run first to differentiate between the grains of copper and silver. It was run at a lower resolution for efficiency, with a longer scan without TruMap enabled run after. Silver had a slightly lower band contrast in EBSPs than copper, leading to a slightly higher mean MAD for silver.

Table 4: Data summary for SEM-EBSD mapping of sample K-21-7, ROI #4, with TruMap enabled.

Phase	Step Size (μm)	Indexed pixels (%)	Mean BC (min/max)	Mean MAD (min/max)
Zero Solutions	6.677	16.96	63.0	N/A
Copper	6.677	74.16	103.5 (37.0/145.0)	0.6222 (0.1168/1.9719)
Silver	6.677	8.88	93.5 (48.0/126.0)	0.9691 (0.2096/1.9811)
Total	6.677	100	95.8 (12.0/145.0)	0.6593 (0.1168/1.9811)

The run time of the second map was 8:32:37. Zero solutions accounted for 9.5% of the sample, with 90.5% total pixels indexed (Table 5). After confirming the identity of the copper and silver grains within this ROI, this map was done to record data with a higher spatial resolution. A smaller step size was chosen in comparison to the previous map for that purpose.

Table 5: Data summary for SEM-EBSD mapping of sample K-21-7, ROI #4, without TruMap enabled.

Phase	Step Size (μm)	Indexed pixels (%)	Mean BC (min/max)	Mean MAD (min/max)
Zero Solutions	2.727	9.5	56.3	N/A
Copper	2.727	90.5	120.1 (24.0/172.0)	0.5394 (0.1073/1.9923)
Total	2.727	100.0	114.1 (7.0/178.0)	0.5394 (0.1073/1.9923)

3.2.3.2   Texture and Microstructure

The copper has experienced significant deformation, similar to ROI #10. Copper grains are 500µm or larger, with most grains showing only one edge boundary on the map (Figure 20B). Copper twinning is seen within the site once more, with twins from ~100µm long and ~5µm wide. These copper twins exhibit ~60° of rotation about the -111 axis compared to the main body of the copper (Figure 20C).
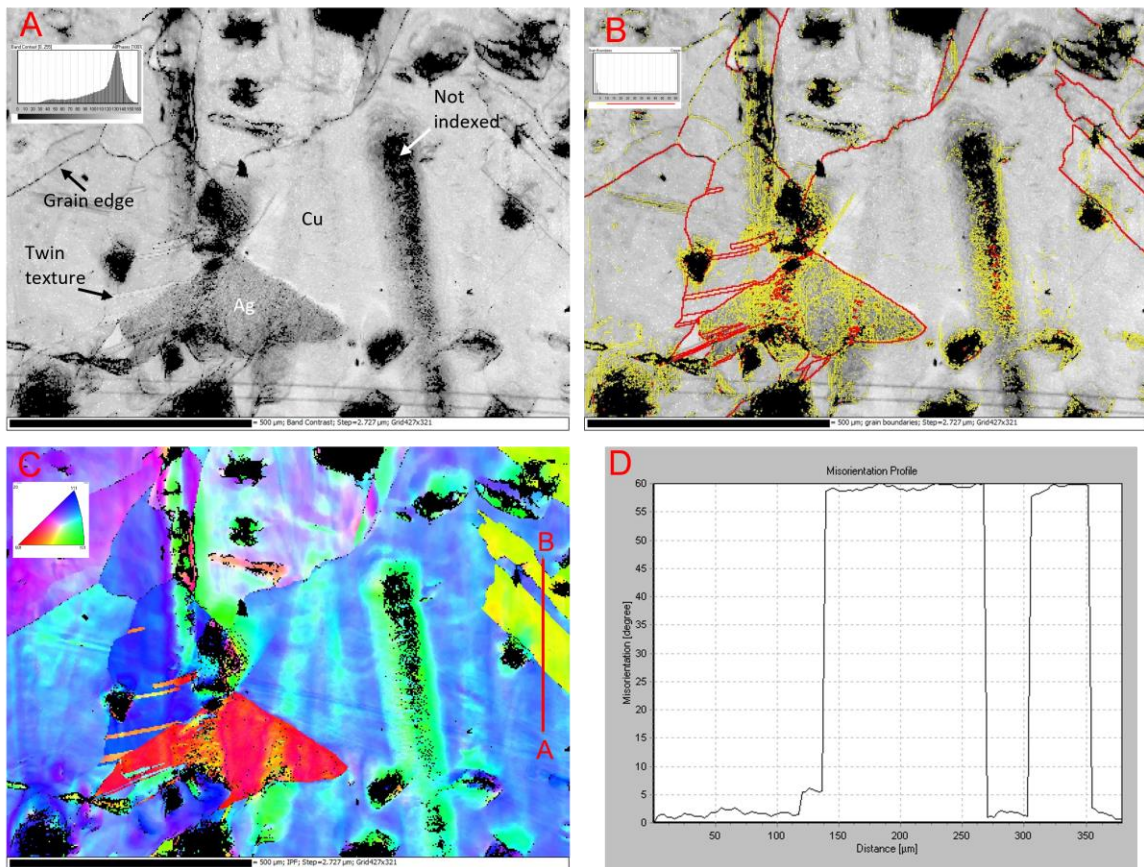
Figure 20: Map images of band contrast (A), edge contrast (B), and inverse pole figure colouration (C) for sample K-21-7 at region of interest #4, from the second run without TruMap enabled. D) misorientation profile of section A-B in image (C). Black pixels in A, B, and C represent locations with zero solutions that were not indexed.

The silver domain of ~500µm shares a similar pattern of deformation. The crystallographic orientation of the silver is close to that of the host copper, it exhibits

domains of plastic deformation of ~5-10°, like the copper. The deformation microstructures seen within the copper carry into the silver (Figures 20C, 21C). A twin is also seen within the silver domain.
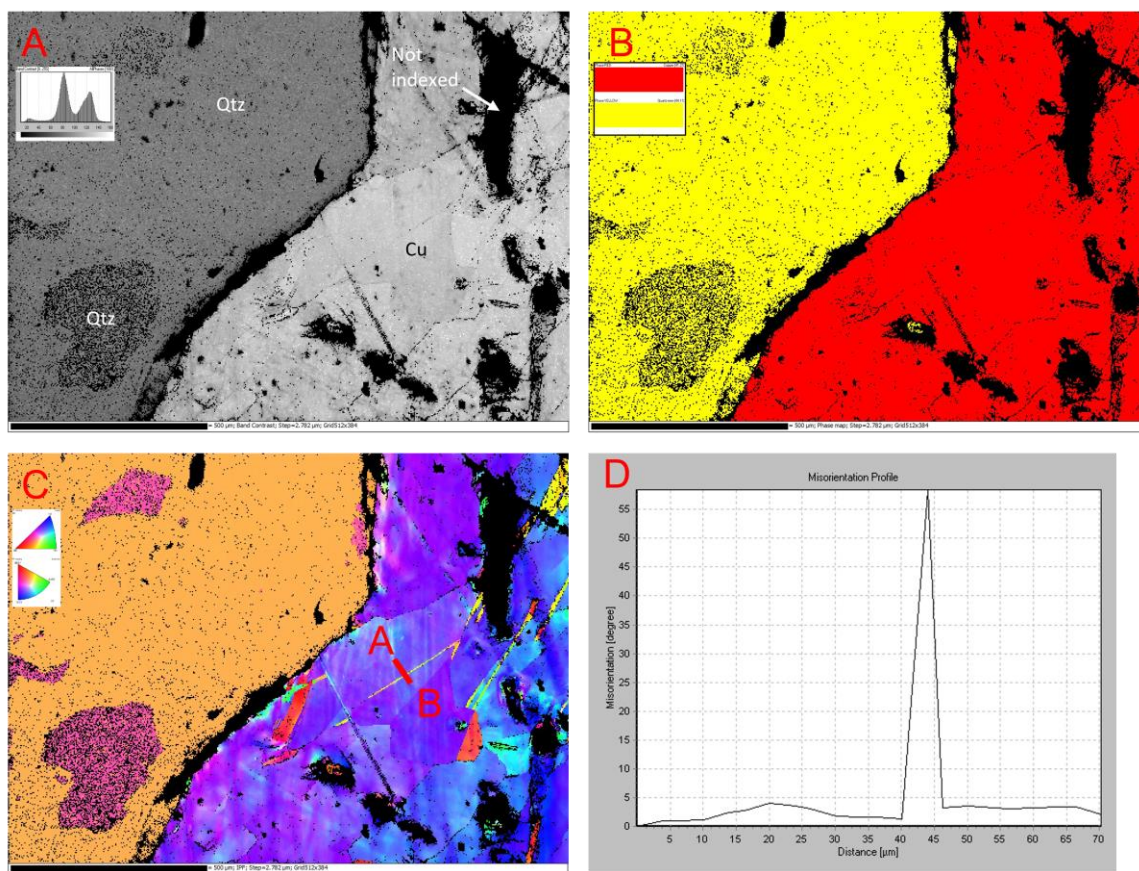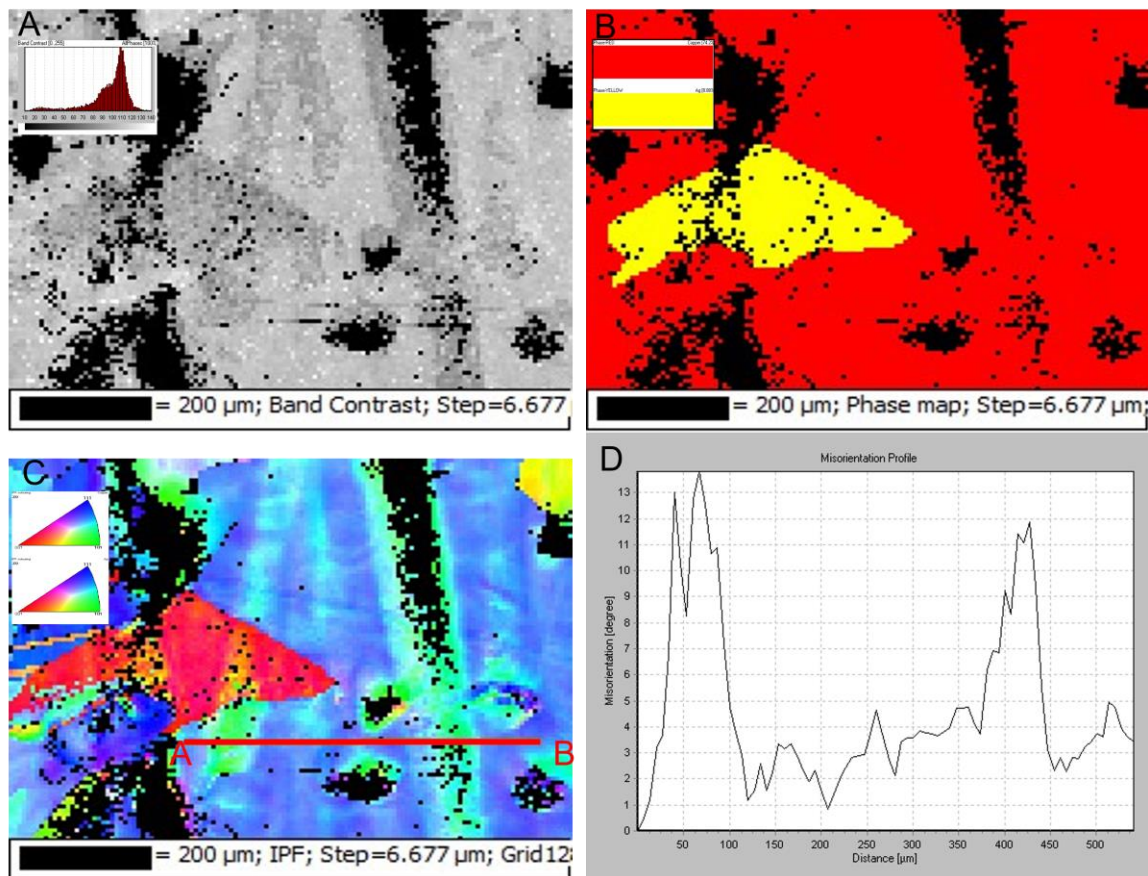

Figure 21: Map images of band contrast (A), phase maps (B), and inverse pole figure colouration (C) for sample K-21-7 at region of interest #4, from the first run with TruMap enabled. D) misorientation profile of section A-B in image (C). Black pixels in A, B, and C represent locations with zero solutions that were not indexed.

3.3 MicroCT

The microCT technique was applied to explore its potential for non-destructive imaging of the interface between copper and its host rock, and of inclusions of other phases of different density within the copper. This had not been done, to the best of my knowledge, on such samples. Nor has this microCT for copper been integrated with SEM-EDS data from the same sample.

An initial microCT scan was done without any filtering to examine the impacts of beam shadowing around the high-density domains (e.g. copper) in the sample. Whereas beams could penetrate some thinner parts of the high-density zones, there were shadowed zones surrounding any large (2+mm) high-density regions within the sample (Figure 22A, B). These data were compared against a scan done with the highest-strength filter to target the high-density materials with the BR6 filter (Figure 22C, D).
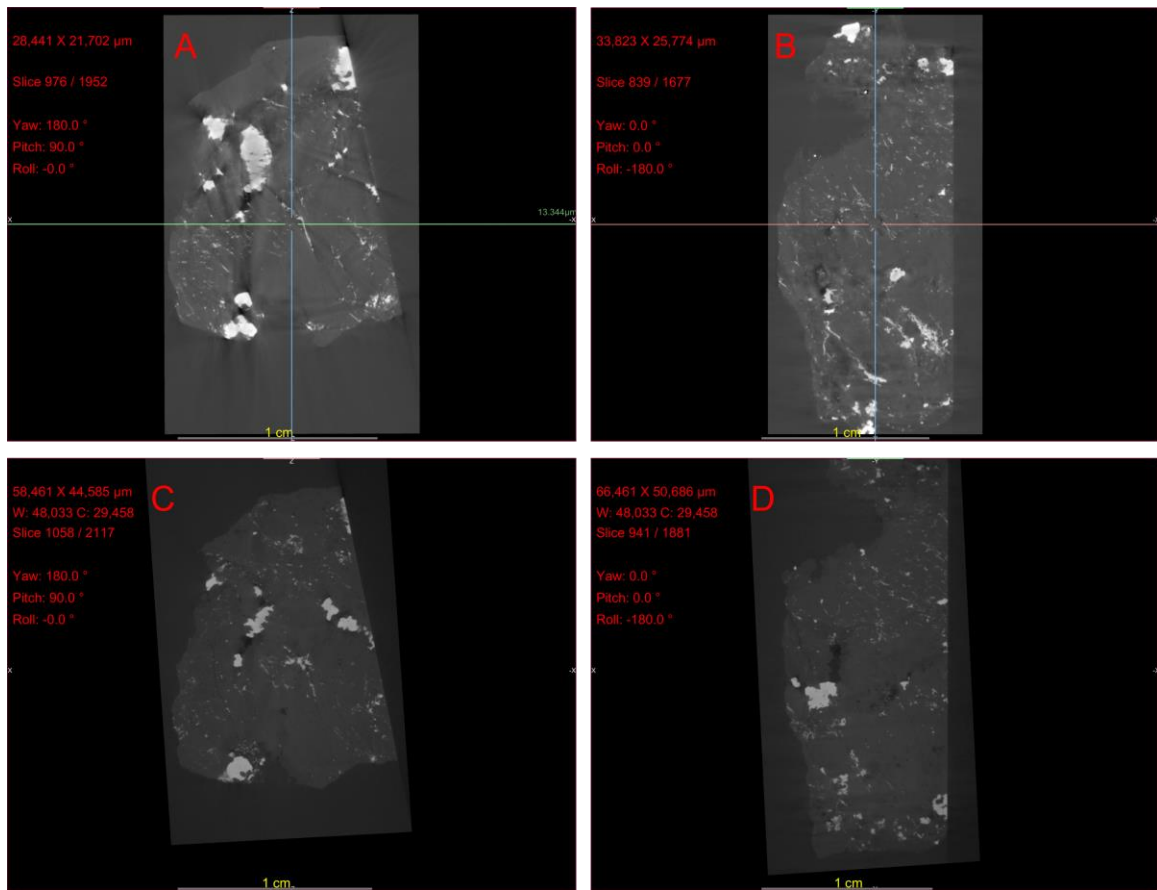
Figure 22: MicroCT "slice" images of the sample with air (A, B) and BR6 (C, D) as filters. The top images have a higher level of contrast, however beam hardening from the copper deposits leaves "streaks" of shadowing throughout the images that is not seen in the BR6 filtered images.

The low-density materials that were targeted in the air scan (Figure 22A, B) showed subtle amounts of contrast in regions that were not obscured due to the shadowing effects. This contrast was not seen in later filtered scans, which were set up to remove the lower-energy X-rays from the spectra resulting in a more monochromatic beam. Shadowing was far less noticeable in the BR6 scan, with the higher energy beams and a longer run time allowing for better penetration of the high-density materials (Figure 22C, D).

A method modification that was explored to offset the impacts of beam shadowing on the no-filter scan was to take a second scan at a different angle and to stitch the two datasets together. This was done with Dragonfly using the stitch 3D datasets tool. While each scan had significant beam shadowing, there was a clear decrease in shadowing effects once the two datasets were stitched (Figure 2).
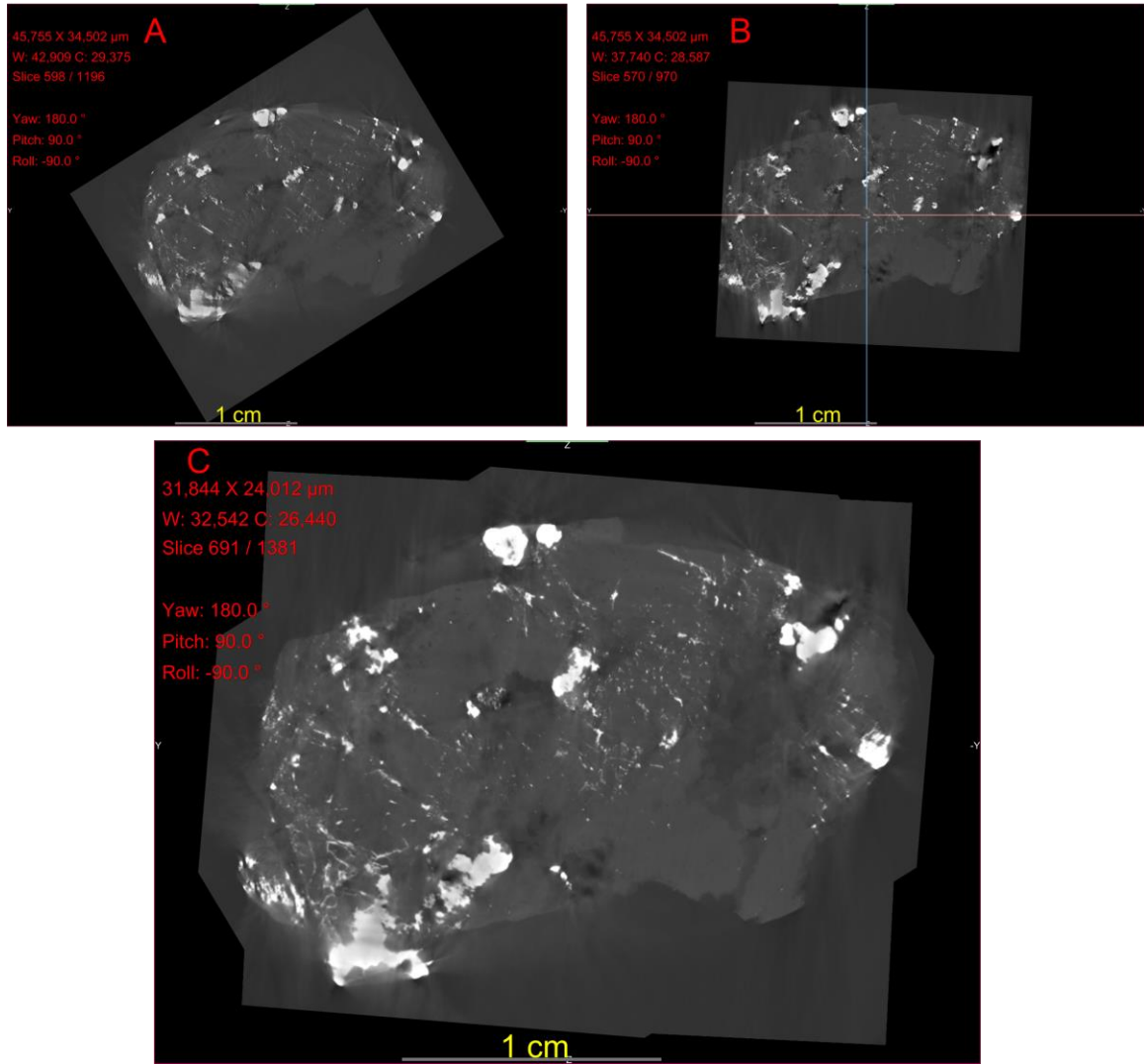
Figure 23: Comparison of scans taken in a vertical (A) and horizontal (B) sample orientation. Shadowing effects from beam hardening are aligned in differing directions. The stitched dataset (C) still shows some shadowing effects, but there is improved visibility compared to either individual scan.

To accomplish this stitching, the intensity profiles of each scan had to be normalized. The pre- and post-normalization intensity histograms can be seen below (Figure 24).
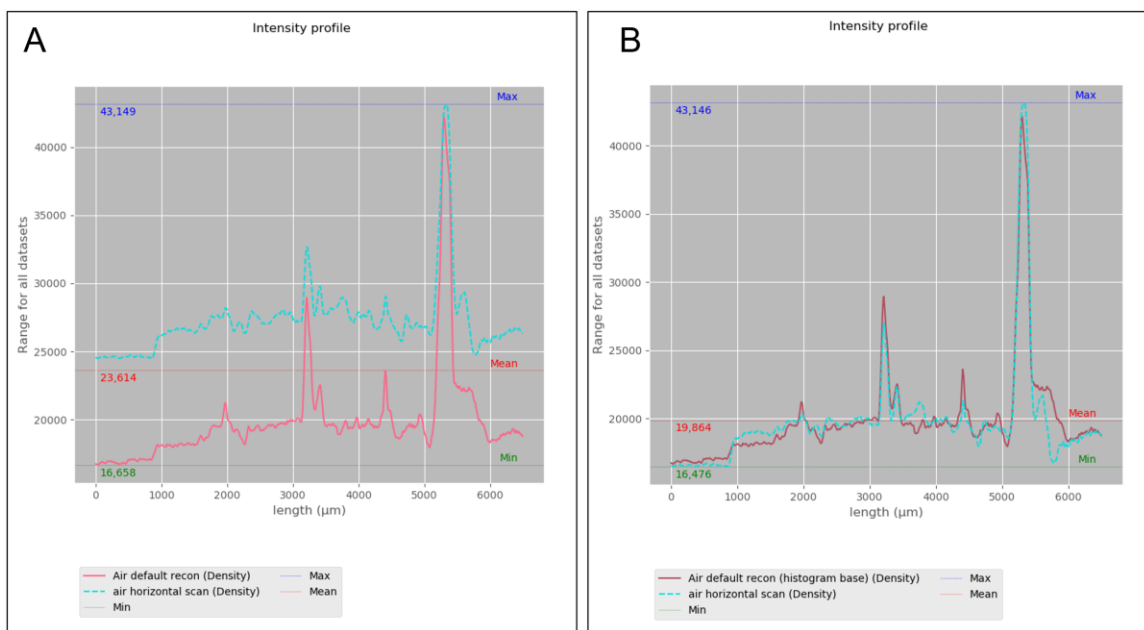
Figure 24: A) Intensity profiles for the two air microCT scans prior to histogram normalization. B) Intensity profiles for the two air microCT scans following histogram normalization.

The three-dimensional (3D) models were produced automatically by the Dragonfly software while importing the imaging files from our microCT scans. After digitally clipping away the histogram values of the low-density materials, the distribution of copper throughout the sample can be seen. Minor colour variations in the copper (purple in Figure 25B) may be due to variations in the shape and size of individual copper blebs, resulting in slightly differing levels of X-ray beam absorption by copper throughout the sample. Some regions of significantly higher density stood out (e.g. white zones in Figure 25B). These zones correlate with a higher density material, possibly a phase like the silver that was found in the SEM scan.
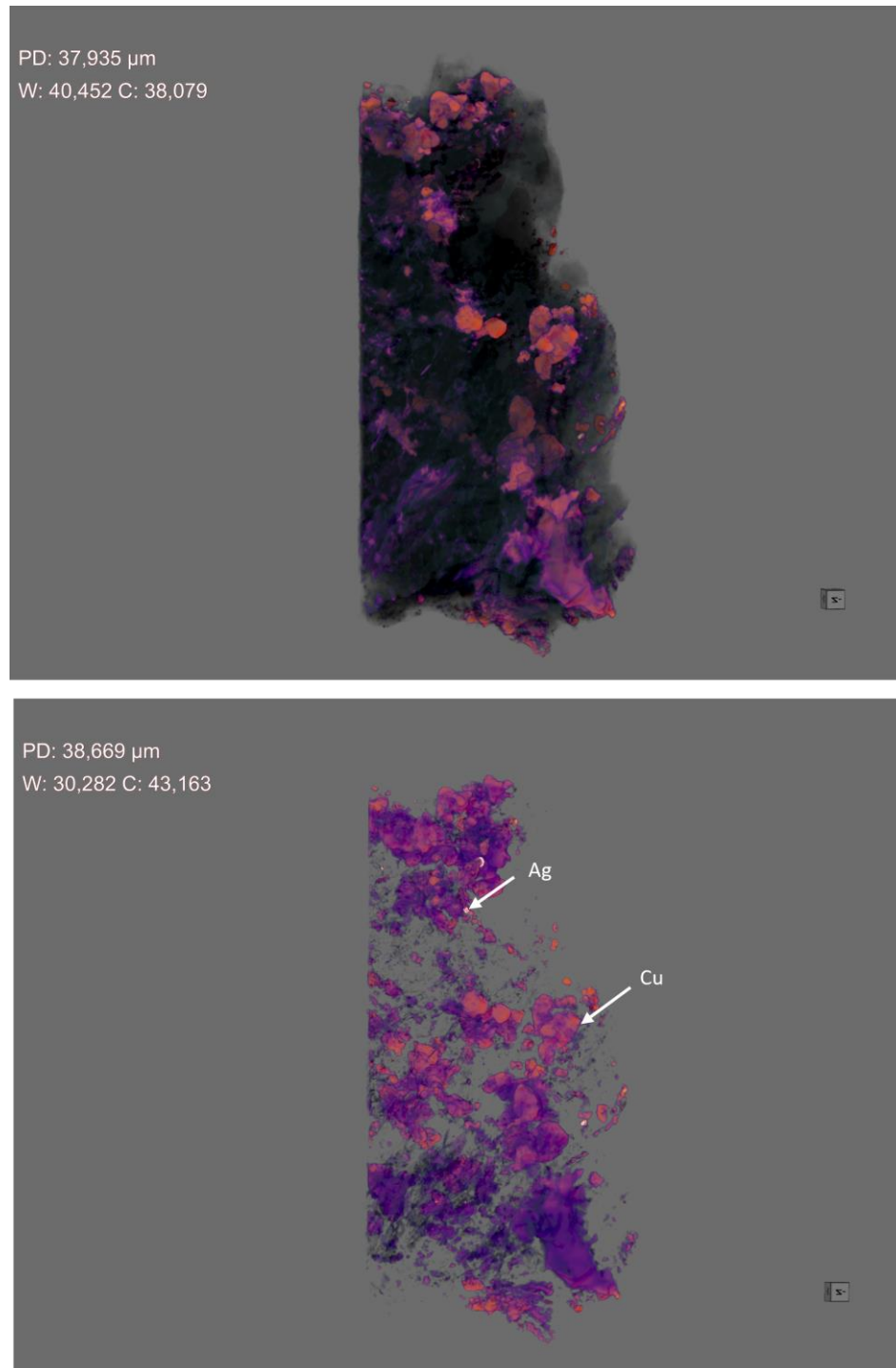
Figure 25: MicroCT 3D models of the BR6 scan. (B) has the low-density minerals clipped from view, revealing some high-density phases (seen in white) that would otherwise not be visible.

By isolating the view parameters, the distribution of the high-density materials throughout the sample can be seen well in the 3D model. The phase is primarily found in one main form as small rounded blebs within and adjacent to the copper.

Chapter 4

4   Discussion

The information gained on copper crystallization history and deformation, and the usefulness of the analytical workflow used to gain this information, are discussed below. For the copper history, the SEM-EDS and SEM-EBSD results are first integrated for each of samples K-21-2 (siltstone) and K-21-7 (basalt amygdule). The integration of the SEM-EDS and microCT results for sample K-21-4A are then considered in light of copper and silver distribution. This is followed by a brief consideration of these copper characteristics in the context of previous work. Finally, a review of the analytical techniques is presented in respect to its usefulness for future natural copper studies for spent nuclear fuel repository research.

4.1   SEM-EDS and SEM-EBSD

4.1.1   Sample K-21-2

The characteristics of this sample suggest it was originally associated with the Allouez conglomerate, part of the Portage Lake Volcanic sequence at the Rhode Island mine (Bornhorst & Rose, 1994). The introduction of hydrothermal fluids post-deposition resulted in the epidote alteration that is seen in some portions of the sample. The epidote and quartz grains have much larger grain sizes than that of the siltstone host, with copper only seen in association with the altered regions. Based on the mineral textures, the copper would have formed latest in the crystallization sequence, surrounding already formed quartz and epidote grains.

There is little evidence for post-crystallization deformation of the copper. The highly deformed zone seen towards the edges of the sample is interpreted to be a result of the preparation process as the deformation is matched along both cut edges of the sample in the plane of the saw cut. On the interior of the sample, there is very little deformation in either the copper or the co-existing quartz crystals. There is some slight plastic deformation near the contacts with harder minerals such as quartz in some locations on

the sample, but sample preparation as a source for this minor deformation cannot be ruled out unequivocally. It may be a result of differential response of these minerals during regional stresses such as the isostatic flexure following glaciations in the area, or it may also be due to the sample's collection history and/or preparation.

4.1.2   Sample K-21-7

This amygdular sample from the Rhode Island mine is similar to features described from the Pewabic lode of the Portage Lake Volcanics (Butler & Burbank, 1929). The K-spar and prehnite in the sample are seen as a result of the copper-bearing hydrothermal fluids which would have travelled through pore spaces in the lode, and would have crystallized after the euhedral quartz grains and K-feldspar grains in the outer regions of the amygdule. The relatively large domain of silver identified near the centre of the sample and main copper body appears to be crystallographically aligned with the copper, and may have co-crystallized from the copper or segregated from known Ag impurities in Keweenaw copper (Mauk et al., 1992; Mauk & Hancock, 1998) at a later stage.

There are significant amounts of deformation and mechanical twinning throughout sample K-21-7 (Figure 20C). Copper is known to be resistant to mechanical twinning, and twins are experimentally induced at strain rates of 10^{-1} or higher (Cronje et al., 2013). These would be extreme relative to strain rates of geological processes (10^{-6} to 10^{-12}) outside of meteorite impact shock waves. There is no reported evidence of shock metamorphism on the Keweenaw district after more than a century of petrographic observation (e.g. Pumpelly, 1871). A simpler explanation is that this sample, which was likely retrieved from a mine dump, has experienced high strain rates during the extraction process. One can also see mechanical twins in the natural silver domain showing that it was exposed to the same, late, high strain event(s). The microstructures are interpreted as being due to sample processing during mining, rather than any geological events. This interpretation is consistent with reports that basalt-hosted copper was processed with large-scale milling and crushing operations (T. Bornhorst, pers. Comm. 2022,). Annealing twins can also be induced as a result of raised temperatures on FCC metals that have limited room for expansion (Mahajan et al., 1997). This method of twinning

was not investigated as a potential source of the deformation at this time, and should also be considered in future works.

4.2   SEM-EDS and microCT

4.2.1   Sample K-21-4A

Sample K-21-4A is likely a vein deposit sample from the Ojibway mine. A possible source would be the Kearsarge amygdaloid, the most productive copper lode in the region (Nicholson, 1995). It was the first sample prepared for SEM-EBSD and the polishing conditions did not produce sufficiently strong diffraction for analysis, so only the SEM-EDS results are considered here. The sample is made up primarily of prehnite, with quartz and copper infilling vein and pore spaces. The oscillatory Fe zoning observed (Figure 9) is similar to that noted in prehnite produced from metasomatic processes from the Miravalles geothermal field, Costa Rica (Yardley et al., 1991). Within pore spaces in the sample, quartz shows euhedral crystal habits, suggesting it began crystallizing prior to the copper. Silver was also noted within this sample and would have a late-stage crystallization or exsolution origin as with the silver in the amygdular copper (above).

This sample was selected for MicroCT analysis for its broad distribution of copper, as well as inclusions of silver. Silver's higher density than copper means that it can be distinguished throughout the mass of the sample. While MicroCT analysis techniques do not provide elemental information, it becomes quite valuable when used in tandem with the SEM-EDS work. With the ability to image the sample interior, we are able to identify regions of interest that would otherwise not be known, such as the high-density domains throughout the sample that we believe correlates to silver. Tracing these high-density domains may give insight into the formation habits of the silver in relation to copper.

4.3   Copper History

Two stages of Keweenaw copper mineralization, one hydrothermal but pre-regional deformation and one post-deformational, have been reported (Mauk et al., 1992) from the White Pine area. However, the post-deformation copper is thought to be restricted to this area (Bornhorst & Barron, 2013). Our results are, on their own, not useful in

discriminating between these mineralization episodes, but since the samples are far from the White Pine district it is most likely that these are part of the main period of mineralization dated at roughly 1.06 Ga (see summary in Gallagher et al., 2017). The copper crystallized during post-depositional metamorphism under prehnite-pumpellyite facies conditions from reduced fluids very low in sulphur, as illustrated in the textures of sample K-21-4A. The paragenesis of the silver is beyond the scope of this thesis. However, at this point, given that there is no evidence for post-copper metamorphism, the silver may have crystallized from the same fluids late in the copper growth process. The integration of SEM-EDS and microCT work on sample K-21-4A makes it possible to identify and measure silver deportment in large samples to further assess the relationship with copper deposits.

This first data on the orientation microstructure (texture) of natural copper establishes that the grain size of the copper is mm-scale, and much larger than the ~50μm scale grains common to electrodeposited manufactured copper planned for use by NWMO. It is premature to make a general statement on natural deformation processes recorded by the copper due the small number of samples, however it is apparent that the mining-induced copper deformation exists, and that this must be taken into account in future work.

4.4   Review of effectiveness of the analytical techniques

Of the three techniques used in this study, two of them, SEM-EBSD and microCT, have not, to the best of our knowledge, been applied to natural copper. Below is a brief review of the suitability of these techniques for future copper analogue work.

Overall, the SEM-EDS method was highly effective in mineral identification in this section and mapping major element gradients. It was possible to narrow down mineral identities within the sample and confirm the presence of phases such as silver. Whereas SEM-EDS element mapping alone is not sufficient to describe the mineralogy, it provided us with the ability to look for regions of interest to target with SEM-EBSD. As well, SEM-EDS mapping was used in tandem with SEM-EBSD in the TruMap function for the first time in the ZAPLab, such that we can now identify minerals in the sample with both chemical and crystallographic information.

The SEM-EBSD method shows great promise for assessing the deformation history of natural copper. As mentioned, when used in tandem with SEM-EDS, it allows for confirmation of minerals based off elemental and structural information. As well, we developed a polishing protocol that allows measurement of the orientation microstructure of metals and host silicates simultaneously. The discovery of mining-induced deformation in this early study has also highlighted the importance of provenance control on samples before investing in a larger body of analytical work. Features such as grain size were also able to be identified using SEM-EBSD, which may be of eventual interest to the NWMO for canister design. There is no previously available SEM-EBSD information for copper samples from the Keweenaw Peninsula, and this research has begun the investigation of its strain history.

The application of microCT to a copper-bearing vein was successful in proving the technology's usefulness in identifying form and heterogeneity of copper deposits. While the resulting 3D models may only display density information, it yields insight into opaque regions in the sample. The shape and distribution of copper deposits within the sample can aid in interpretations of crystallization. As well, protocols were developed to allow for the identification of higher density materials such as the silver within dense copper veins, features that would otherwise be completely hidden. Future work to test the effectiveness of these methods would include further cutting a sample once one of these high-density regions has been identified, to make an attempt to then re-analyze the interior surface with SEM-EDS and SEM-EBSD to confirm the identity of these high-density phases.

This project has shown the value of combining multiple measurement techniques to characterize natural copper and co-existing minerals in a novel way. Developing a workflow for utilizing multiple imaging techniques has been done with careful sample preparation techniques and epoxy mounting, allowing for both 2D and 3D imaging of irregularly shaped samples (Figure 26).
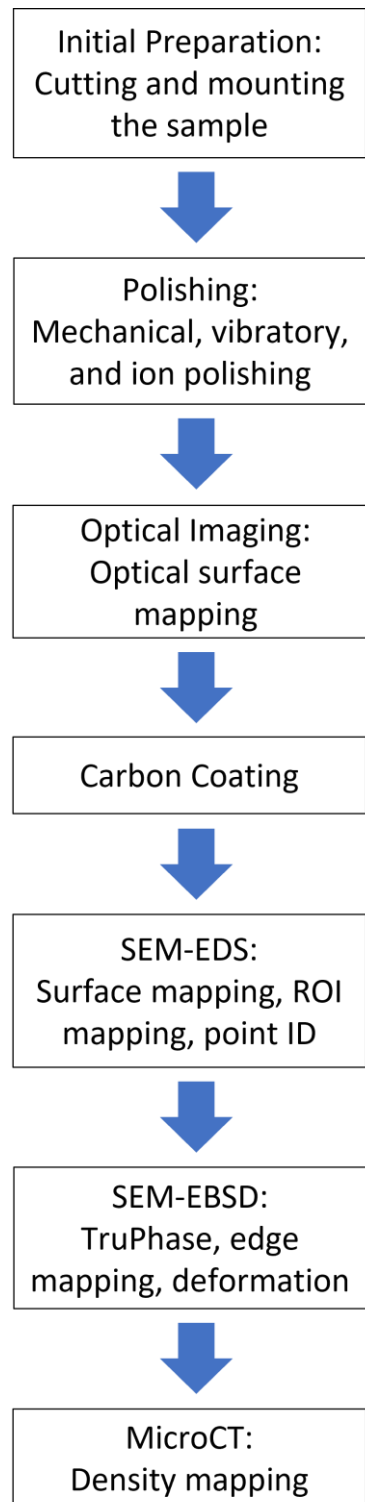
Figure 26: Outline of the workflow developed in this study.

Future work on natural copper as an analogue for copper container coatings of spent nuclear fuel can apply and refine the workflow. Additional methods to understand the relationship of copper and silver crystallization may require additional techniques such as laser multi-collector ICPMS and atom probe. Samples characterized in this study can now be investigated by corrosion chemists in the collaborating research group at Western University, furthering the suite of knowledge to be gained from any one sample. Future work could include developing collaborative relationships with Indigenous knowledge holders in the Great Lakes region and exchanging knowledge on copper. This was not possible during this study due to Covid-19 travel and community restrictions.

Chapter 5

5   Conclusion

In conclusion, this study showed the effectiveness of combining multiple imaging types for the characterization of natural copper samples hosted by other minerals. By using a suite of imaging techniques, we are able to obtain layers of data in both 2D and 3D that would not be possible using only one method. Further refinement of this workflow will allow for the efficient characterization of many natural irregularly shaped samples, which can then be investigated by the collaborating corrosion chemists at Western University.

This study demonstrates the effectiveness of combining electron and X-ray microscopy techniques to effectively characterize natural analogues for use in DGR research. Even at a micrometre scale, there was no evidence of corrosion (secondary mineral formation) in or on the margins of these copper domains after 1 billion years in the Great Lakes region. This supports the value in studying Keweenawan copper in understanding the properties of copper that avoids corrosion over geologic timescales.

Details such as grain size, silver content, and strain history can be used in the future to inform DGR design and planning by the NWMO's scientists. These samples which have been characterized can now also be studied by collaborating corrosion chemists at Western University for use in further electrochemistry and corrosion studies. To the best of our knowledge, this thesis is the first application of these techniques (particularly SEM-EBSD) on Keweenawan copper in over 150 years of geological research on the region.

References

Abrahamsen-Mills, L. & Small, J. (2019). *State of Science Review: Modelling microbial effects to assess long-term performance of a DGR.* (Nuclear Waste Management Organization Report NWMO-TR-2019-15). Nuclear Waste Management Organization. https://www.nwmo.ca/~/media/Site/Reports/2019/12/03/19/17/NWMOTR201915--State-of-Science-Review-Modelling-microbial-effects-to-assess-longterm-performance-of-a-DGR.ashx?la=en

Bebber, M. R., Key, A. J. M., Fisch, M., Meindl, R. S., & Eren, M. I. (2019). The exceptional abandonment of metal tools by North American hunter-gatherers, 3000 B.P. *Scientific Reports (9),* 5756.

Bornhorst, T. J. (1997). Tectonic Context of Native Copper Deposits of the North American Midcontinent Rift System. *Geological Society of America, Special Paper 312.*

Bornhorst, T. J., & Barron, R. J. (2013). Field Trip Guidebook. *Institute on Lake Superior Geology Proceedings, 59(2).*

Bornhorst, T. J., & Mathur, R. (2017). Copper Isotope Constraints on the Genesis of the Keweenaw Peninsula Native Copper District, Michigan, USA. *Minerals, 7(10),*185.

Bornhorst, T. J., & Rose, W. I. (1994). Self-Guided Geological Field Trip to the Keweenaw Peninsula, Michigan. *Institute on Lake Superior Geology Proceedings, 40(2),* 185.

Bornhorst, T. J., Paces, J. B., Grant, N. K., Obradovich, J. D., & Huber, N. K. (1988). Age of Native Copper Mineralization, Keweenaw Peninsula, Michigan. *Economic Geology, 83,* 619-625.

Brown, A. C. (2006). Genesis Of Native Copper Lodes in The Keweenaw District, Northern Michigan: A Hybrid Evolved Meteoric and Metamorphogenic Model. *Economic Geology, 101,* 1437-1444.

Butler, B. S., & Burbank, W. S. (1929). *The copper deposits of Michigan.* (Professional Paper 144). United States Geological Survey. https://doi.org/10.3133/pp144

Buyers, J. (2022). *Characterization of the Mineralization and Corrosion of Natural Copper from the Keweenaw Peninsula, Michigan.* [Unpublished Bachelor's thesis]. University of Western Ontario.

Chisambi, J., von der Heyden, B., Tshibalanganda, M., & Le Roux, S. (2020). Gold Exploration in Two and Three Dimensions: Improved and Correlative Insights from Microscopy and X-Ray Computed Tomography. *Minerals, 10(5),* 476.

Cronje, S., Kroon, R. E., Roos, W. D., & Neethling, J. H. (2013). Twinning in Copper Deformed at High Strain Rates. *Bulletin of Materials Science, 36(1),* 157-162.

Davis, D. W., & Paces, J. B. (1990). Time Resolution of Geologic Events on the Keweenaw Peninsula and Implications for Development of the Midcontinent Rift System. *Earth and Planetary Science Letters, 97,* 54-64.

Gohman, S. M. (2013). It's Not Time to Be Wasted: Identifying, Evaluating, and Appreciating Mine Wastes in Michigan's Copper Country. *The Journal of the Society for Industrial Archeology, 39 (1)*, 5-22.

Natural Resources Canada. (2021). *Energy Fact Book.* https://www.nrcan.gc.ca/sites/nrcan/files/energy/energy_fact/2021-2022/PDF/2021_Energy-factbook_december23_EN_accessible.pdf

Fayek, M., & Brown, J. (2015). *Natural and Anthropogenic Analogues for High-Level Nuclear Waste Disposal Repositories: A Review.* (Canadian Nuclear Safety Commission Report RSP-310). Canadian Nuclear Safety Commission. http://www.nuclearsafety.gc.ca/eng/pdfs/Natural-Analogues-Final-Report.pdf

Gallagher, T. M., Sheldon, N. D., Mauk, J. L., Petersen, S. V., Gueneli, N., & Brocks, J. J. (2017). Constraining the Thermal History of the North American Midcontinent Rift System using Carbonate Clumped Isotopes and Organic Thermal Maturity Indices. *Precambrian Research, 294,* 53-66.

Green, J. C. (1983). Geologic and Geochemical Evidence for the Nature and Development of the Middle Proterozoic (Keweenawan) Midcontinent Rift of North America. *Tectonophysics, 94,* 413-437.

Hall, D. S., & Keech, P. G. (2017). An overview of the Canadian corrosion program for the long-term management of nuclear waste. *Corrosion Engineering, Science and Technology, 52(1),* 2-5.

Jeong, J., Urban, N. R., & Green, S. (1999). Release of Copper from Mine Tailings on the Keweenaw Peninsula. *Journal of Great Lakes Research, 25(4),* 721-734.

Kerfoot, W. C., Urban, N., Jeong, J., MacLennan, C., & Ford, S. (2020). Copper-rich "Halo" off Lake Superior's Keweenaw Peninsula and how Mass Mill tailings dispersed onto tribal lands. *Journal of Great Lakes Research, 46(5),* 1423-1443.

Mahajan, S., Pande, C. S., Imam, M. A., & Rath, B. B. (1997). Formation of Annealing Twins in F.C.C. Crystals. *Acta Materialia, 45(6),* 2633-2638.

Mauk, J. L., & Hancock, R. G. V. (1998). Trace Element Geochemistry of Native Copper from the White Pine Mine, Michigan (USA): Implications for Sourcing Artifacts. *Archaeometry, 40(1),* 97-107.

Mauk, J. L., Kelly, W. C., van der Plujim, B. A., & Seasor, R. W. (1992). Relations Between Deformation and Sediment-Hosted Copper Mineralization: Evidence from the White Pine of the Midcontinent Rift System. *Geology, 20(5),* 427-430.

Mitchell, R. L., & Sheldon, N. D. (2016). Sedimentary Provenance and Weathering Processes in the 1.1 Ga Midcontinental Rift of the Keweenaw Peninsula, Michigan, USA. *Precambrian Research, 275,* 225-240.

Mohd Tadza, M. Y., Mohd Tadza, M. A., Bag, R., & Harith, N. S. H. (2018). Potential impact of Andrassy bentonite microbial diversity in the long-term performance of a deep nuclear waste repository. *IOP Conference Series: Materials Science and Engineering, 298*.

National Park Service. (2022a, June 8). *Environmental Impacts of Mining in the Keweenaw.* https://www.nps.gov/kewe/learn/nature/environmental-impacts-of-mining-in-the-keweenaw.htm

National Park Service. (2022b, June 5). *Timeline of Michigan Copper Mining 1951 to Present.* https://www.nps.gov/kewe/learn/historyculture/copper-mining-timeline-page-4.htm

National Park Service. (2022c, May 28). *Timeline of Michigan Copper Mining Prehistory to 1850.* https://www.nps.gov/kewe/learn/historyculture/copper-mining-timeline.htm

Nicholson, S. W. (1992). *Geochemistry, Petrography, and Volcanology of Rhyolites of the Portage Lake Volcanics, Keweenaw Peninsula, Michigan.* (U.S. Geological Survey Bulletin 1970B). https://pubs.er.usgs.gov/publication/b1970AB

Nicholson, S. W. (1995). *Kearsarge Amygdaloid.* United States Geological Survey. https://mrdata.usgs.gov/mrds/show-mrds.php?dep_id=10082605

Nicholson, S. W. (1997). *Allouez Conglomerate Lode.* United States Geological Survey. https://mrdata.usgs.gov/mrds/show-mrds.php?dep_id=10082609

Nuclear Waste Management Organization (2021). *What is Used Nuclear Fuel?* https://www.nwmo.ca/~/media/Site/Files/PDFs/2021/03/15/20/45/Backgrounder-2021-What-is-used-nuclear-fuel.ashx

Nuclear Waste Management Organization. (2022). *Radiation Risk and Safety.* https://www.nwmo.ca/en/Canadas-Plan/Canadas-Used-Nuclear-Fuel/Radiation-Risk-and-Safety

Ojakangas, R. W., Morey, G. B., & Green, G. C. (2001). The Mesoproterozoic Midcontinent Rift System, Lake Superior Region, USA. *Sedimentary Geology, 141-142,* 421-442.

Ojibway Mine, Ojibway, Keweenaw Co., Michigan, USA. (2022a). Mindat.org. Retrieved May 14, 2022 from https://www.mindat.org/loc-17167.html

Palacas, J. G., Schmoker, J. W., Daws, T. A., Pawlewicz, M. J., & Anderson, R. R. (1990). Petroleum source-rock assessment of Middle Proterozoic (Keweenawan) sedimentary rocks, Eischeid #1 well, Carroll County, Iowa. *The Amoco M.G. Eischeid #1 Deep Petroleum Test.* 119-134.

Pumpelly, R. (1871). The Paragenesis and Derivation of Copper and its Associates on Lake Superior. *American Journal of Science, 3-2(9),* 188-198.

Redix, E. M. (2017). "Our Hope and Our Protection": Misko-biiwaabik (Copper) and Tribal Sovereignty in Michigan. *American Indian Quarterly, 41(3),* 224-249.

Rhode Island Mine, Boston, Houghton Co., Michigan, USA. (2022b). Mindat.org. Retrieved May 14, 2022 from https://www.mindat.org/loc-33322.html

Rosemeyer, T. (1998). News from the Keweenaw Recent: Mineral Finds in Michigan's Copper Country. *Rocks & Minerals, 73(3),* 182-195.

Rosemeyer, T. (2010). The Pewabic Copper-bearing Amygdaloidal Lode, Houghton County, Michigan Lake Superior Native Copper District. *Rocks & Minerals, 85 (4),* 300-316.

Scully, J. R., Féron, D., & Hänninen, H. (2016). *Review of the NWMO Copper Corrosion Program.* (Nuclear Waste Management Organization Report NWMO-TR-2016-11). Nuclear Waste Management Organization. https://www.nwmo.ca/~/media/Site/Reports/2016/10/13/15/04/NWMO_TR_2016_11.ash x\

Stoiber, R. E., & Davidson, E. S. (1959). Amygdule Mineral Zoning in the Portage Lake Lava Series, Michigan Copper District. *Economic Geology, 54,* 1250-1277

Tribal Lands Program. (N. D.) *Tribes and Hardrock Mining.* https://www.nwf.org/~/media/PDFs/Wildlife/Mining-Loopholes/Tribal_v4/Tribal_v6.ashx

United States Nuclear Regulatory Commission. (2019, July 3). *Backgrounder of radioactive waste.* https://www.nrc.gov/reading-rm/doc-collections/fact-sheets/radwaste.html

Woodruff, L. G., Shulz, K. J., Nicholson, S. W., & Dicken, C. L. (2020). Mineral deposits of the Mesoproterozoic Midcontinent Rift system in the Lake Superior region – A space and time classification. *Ore Geology Reviews, 126.*

Yardley, B. W. D, Rochelle, C. A., Barnicoat, A. C., & Lloyd, G. E. (1991). Oscillatory Zoning in Metamorphic Minerals: an Indicator of Infiltration Metasomatism. *Mineralogical Magazine, 55(380),* 357-365.

Zhang, M., Clark, B., King, A. J., Russell, S. S., & Lin, Y. (2021). Shape and Porosity of Refractory Inclusions in CV3 Chondrites: A Micro-computed Tomography (μCT) Study. *Meteoritics & Planetary Science, 56(3),* 500-514.

Curriculum Vitae

Name: Emilie Landry

Post-secondary   McMaster University
Education and   Hamilton, Ontario, Canada
Degrees: 2015-2020, B.Sc

Related Work   Teaching Assistant
Experience   The University of Western Ontario
                    2020-2021